Titre: Title:	The Impact and Elimination of Carbonaceous Impurities in Chemical Vapor Deposition Graphene on Copper
Auteur: Author:	Dhan Dhananjaya Cardinal
Date:	2018
Type:	Mémoire ou thèse / Dissertation or Thesis
Référence: Citation:	Cardinal, D. D. (2018). The Impact and Elimination of Carbonaceous Impurities in Chemical Vapor Deposition Graphene on Copper [Mémoire de maîtrise, École Polytechnique de Montréal]. PolyPublie. https://publications.polymtl.ca/3761/

URL de PolyPublie: PolyPublie URL:	https://publications.polymtl.ca/3761/
Directeurs de recherche: Advisors:	Patrick Desjardins, & Richard Martel
Programme: Program:	Génie physique

UNIVERSITÉ DE MONTRÉAL

THE IMPACT AND ELIMINATION OF CARBONACEOUS IMPURITIES IN CHEMICAL VAPOR DEPOSITION GRAPHENE ON COPPER

DHAN DHANANJAYA CARDINAL

DÉPARTEMENT DE GÉNIE PHYSIQUE

ÉCOLE POLYTECHNIQUE DE MONTRÉAL

MÉMOIRE PRÉSENTÉ EN VUE DE L'OBTENTION

DU DIPLÔME DE MAÎTRISE ÈS SCIENCES APPLIQUÉES

(GÉNIE PHYSIQUE)

DÉCEMBRE 2018

UNIVERSITÉ DE MONTRÉAL

ÉCOLE POLYTECHNIQUE DE MONTRÉAL

Ce mémoire intitule :

THE IMPACT AND ELIMINATION OF CARBONACEOUS IMPURITIES IN CHEMICAL VAPOR DEPOSITION GRAPHENE ON COPPER

présenté par : CARDINAL Dhan Dhananjaya

en vue de l'obtention du diplôme de : Maîtrise ès sciences appliquées

a été dûment accepté par le jury d'examen constitué de :

M. PETER Yves-Alain, D. Sc., président

M. DESJARDINS Patrick, Ph. D., membre et directeur de recherche

M. MARTEL Richard, Ph. D., membre et codirecteur de recherche

M. STAFFORD Luc, Ph. D., membre externe

DEDICATION

To all past, present and future independent scientists…

And to my mother,

who gave me the world.

ACKNOWLEDGEMENTS

The thank you page is a strange one to write. Often times, and it certainly was for me, it's the first page that you write mentally from the beginning of your academic adventure but the last one to be physically written; its contents shifting and changing as your own moods wane and wax in regard to the people you know you'll include. Ultimately, when you sit down to finally write it, as things come to a close, you have a bit more humility and, hopefully, wisdom, to see things from a bird's eye-view.

I'd like to take this opportunity to thank those around me who made this possible, in no particular order. I want to thank Paul Heroux, for his wisdom and insight, Michael Ashton, for his ears and accepting nature, Linda Walters, for her love, my office, friends and colleagues for putting up with me, and lastly, my mother, for her sacrifices. From an academic perspective, I want to extend my gratitude to my supervisors, Pierre Levesque, for his giving spirit, who gave a lot of himself and his knowledge, Patrick Desjardins, for his time and smile, and Richard Martel, for his charitability and generosity of character, whom gave me a chance when no one else would and saw in me a scientist.

Thank you.

RÉSUMÉ

Grace à ses propriétés uniques, le graphène a réussi à capter l'attention des scientifiques depuis sa première isolation. Les mécanismes de croissance de cet allotrope de carbone ne sont pas entièrement compris mais il est connu qu'ils dépendent du substrat sur lequel est cru ce matériau incroyable. Dans une expérience typique de synthèse de graphène par dépôt chimique en phase vapeur (CVD), le substrat catalyse la dissociation d'un hydrocarbure via deux régimes de croissances possibles : le premier purement surfacique, où le carbone reste lié à la surface pour des métaux de transition ayant une faible solubilité du carbone (Cu et possiblement Pt), le second impliquant une dissolution dans le matériau suivi d'une précipitation du carbone (Ir, Ru, Ni). Dans ces travaux, nous proposons que ce mécanisme dépend d'un seuil, c'est à dire que la solubilité du carbone dans le cuivre est extrêmement faible mais assez haute pour que le carbone présent dans le matériau peut jouer un rôle dans la germination et la croissance latérale du graphène. Cet effet est étudié via le piégeage du carbone grâce à un prétraitement d'oxygène afin de purifier le cuivre ce qui montre les impacts sur la germination du graphène. Nous avons découvert que la méthode de purification la plus efficace est d'induire l'oxydation du cuivre en profondeur dicté par le diagramme de phase Cu-O ce qui nécessite une réduction de température pendant le prétraitement de $1000°C$ a $700°C$ en gardant une pressure d'oxygène de $5x10^{-5}$ Torr. Étendu sur 3 croissances avec un temps de prétraitement augmentant (10, 20, et 40 min) suivi d'un protocole de croissance de graphène normal, la nucléation de graphène est réduite résultant en une augmentation de taille de domaine jusqu'une suppression complète est atteint à 40 min. Un prétraitement d'oxygène nous permet aussi de faire croitre des domaines de graphène large de 860 μm^2

ABSTRACT

Graphene has piqued the interest of scientists and technologists since its isolation because of its unique properties. The growth mechanisms of this carbon allotrope aren't fully understood but are known to depend on the substrate used to grow this wonder material. In a typical graphene synthesis experiment using chemical vapor deposition (CVD), the substrate catalyzes the dissociation of a hydrocarbon with two possible growth regimes: one purely surface mediated where the carbon remains surface-bound for transition metals having very low carbon solubility (Cu and possibly Pt) and one involving a bulk dissolution and subsequent precipitation of the carbon (Ir, Ru, Ni). In this work we propose that the salient feature is one of threshold, that is to say, the carbon solubility of copper is extremely low but is elevated *enough* that bulk-bound carbon can play a role in nucleation and subsequent lateral growth of graphene. This is investigated *via* carbon gettering using oxygen gas pre-treatments to further purify the copper which show clear impacts on graphene nucleation. It was found that the most efficient method of purification is to induce bulk copper oxide as dictated by the Cu-O phase diagram which means lowering the temperature during pre-treatment to $700°C$ from the $1000°C$ growth temperature and maintaining a $5x10^{-5}$ Torr oxygen pressure. Over 3 growths of increasing pre-treatment time (10, 20, and 40 min) followed by a regular graphene growth protocol, the graphene nucleation is reduced resulting in increased single domain size until full quenching is achieved at 40 minutes. An oxygen pre-treatment also enables us to grow large-area graphene domains of 860 μm^2.

TABLE OF CONTENTS

LIST OF TABLES

LIST OF FIGURES

LIST OF SYMBOLS AND ABBREVIATIONS

APCVD	Atmospheric Pressure Chemical Vapor Deposition
BO	Backside Oxide
BSE	Backscattered Secondary Electrons
CVD	Chemical Vapor Deposition
DFT	Density Functional Theory
FWHM	Full-Width Half-Maximum
HOPG	Highly Oriented Pyrolytic Graphite
LPCVD	Low Pressure Chemical Vapor Deposition
MFC	Mass-Flow Controller
ML	Monolayer
OF	Oxygen-Free
OR	Oxygen-Rich
PMMA	Poly(Methyl Methacrylate)
Ppm	parts per million
Ppb	parts per billion
Sccm	Standard cubic centimeter per minute
SE	Secondary Electrons
SEM	Scanning Electron Microscope
TOF-SIMS	Time-of-Flight Secondary Ion Mass Spectrometer
UHP	Ultra High Purity
XPS	X-ray Photoemission Spectroscopy

LIST OF APPENDICES

CHAPTER 1 INTRODUCTION

1.1 Graphene: A Decade Later

Graphene was first studied as reduced graphite oxide in 1859 for its highly lamellar structure by B. C. Brodie[1] followed by theoretical work on its electronic properties in 1947 by P. R. Wallace[2] out of which would emerge the massless Dirac fermion equation modeling the behavior of its electrons.[3] In spite of its relatively recent isolation in 2004, it quickly garnered a Nobel prize for the researchers responsible for this feat in 2010, Konstantin Novoselov and Andre Geim. They were able to do this *via* micromechanical cleavage, or more simply put, using scotch tape to remove layers from highly-oriented pyrolytic graphite (HOPG) until a single layer was obtained.[4] Therefore, in its simplest terms, graphene can be defined as a single-atom-thick sheet of carbon which are bonded to one-another hexagonally. Since then, graphene has taken the world by storm with some musing that it can do everything… except leave the lab.

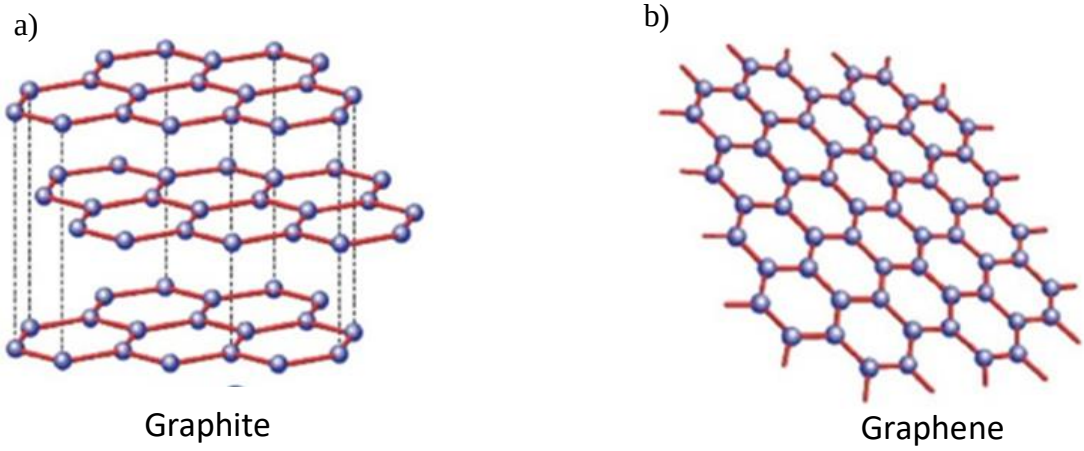

Figure 1-1 Stick and ball model of (a) graphite and (b) graphene clearly showing that graphite is composed of multiple layers of graphene. Reproduced with permission from ref. 4. Nature publishing group, copyright 2010.

It's difficult to know whether graphene has surpassed the collective expectations of the scientific community 14 years after its isolation. When looking at its far-reaching applicability such as: transistors,[5] energy storage devices,[6] electrodes,[7] electrically conductive inks,[8] reagent in composites[9] and sensors[10] we seem to be more limited by our imaginations than anything else. This isn't to suggest that graphene can do *everything*, for example, it will never replace silicon transistor technology without modifications due to it's semi-metal band-gapless nature,[11] but rather, that it might be able to do *something in everything*. This excitement surrounding graphene is mainly due to its amazing properties: a room temperature thermal conductivity twice that of the next best,

diamond, up to $\sim 5000\, W\, m^{-1}K^{-1}$[12], a Young's modulus higher than steel ($\sim 1\, TPa$),[13] nearly transparent, absorbing only $\sim 2.3\%$ of white light[14] as well as an ability to recover its electrical properties upon bending and unbending.[15]

1.1.1 Chemical Vapor Deposition of Graphene on Copper

However, exploiting these properties for technological advancement, as opposed to purely research-oriented purposes, requires an ability to produce graphene on an industrial scale. Originally isolated via graphite exfoliation in 2004[11] yielding flakes of an uncontrollable size and dimension with the added complication of locating them, researchers quickly honed in on synthesizing this atomically flat carbon allotrope via chemical vapor deposition (CVD).[15] First done on nickel in 2008[16] based off of work done on the Ni-C system between the late 70's to mid 80's,[17] it took a full year for it to finally be done on copper.[18] Both of these substrates – copper with its surface-mediated regime and nickel with the bulk playing a predominant role – opened the doors to producing this wonder material on a large scale, limited by substrate or reactor size.

The first reported growth of graphene on copper was done by low pressure CVD (LPCVD) using methane (CH_4) as the carbon precursor and molecular hydrogen as a reducing agent and carrier gas.[18] The copper was held at $1000°C$, below it's melting temperature of $1060°C$, at a low methane and hydrogen pressure (~540 mTorr total) for 5-45 minutes. Extensive research in every aspect of graphene synthesis, ranging from using atmospheric pressure CVD (APCVD) which has demonstrated a different growth regime,[19] to using different types of carbon precursors,[20] and studies involving the role of hydrogen[21] as well as the impact of temperature on the synthesis.[22]

Growing graphene on copper instead of nickel simplified the process by eliminating the need to control cooling rate since it is *via* this mechanism of carbon saturation and subsequent precipitation upon cooling that graphene on nickel is possible. Rather, due to a low carbon solubility, the kinetics of carbon on copper is limited to being surface mediated. To give a general overview of the process, upon introduction of a carbon-containing gas, such as a hydrocarbon, the copper surface is responsible for the catalytic dissociation of the precursor molecule. The adsorbed carbon atom (adatom) mobility is then simply dictated by the temperature whereupon, eventually, enough carbon atoms conglomerate to form a nucleation center, at which point graphene grows 2-dimensionally.

1.2 Objectives of the Present Work

Graphene is interesting to many different fields for many different reasons. From an engineering point of view, a sensitivity for fundamental crystal growth is particularly important as this plays a role in the, broadly speaking, quality, but more precisely, optical, electrical and mechanical properties, in a way where these become, hopefully and ultimately, controllable. From the outset of this project we aimed to gain a better understanding of the parameters that affected:

I. nucleation – fundamental to understanding graphene growth, generally, but also, it's impact on;
II. size of the individual graphene grains, which opens up its potential scientific and technological applications and;
III. number of layers, which impacts its above-mentioned properties.

Proceeding from an otherwise normal graphene synthesis following an oxygen pre-treatment (which will all be elaborated upon later on), what we found was these three things depended heavily on the copper substrate in an unexpected way. It's a well-known fact that the carbon solubility of copper is one of the lowest of the transition metals which made it *seem* obvious that the only growth parameters at play would be surface-related ones. The question that we attempted to answer was not whether there could be carbon in the copper substrate given its minute but non-zero solubility, rather, whether there could be *enough* carbon impurities in copper to play a role in graphene growth. Of note is the fact that the copper that was used in all our growths was $25\mu m$ thick Alfa-Aesar 99.8% metal-basis purity. This foil, being cold-rolled to its desired thickness, is theorized to have carbon impurities added from its industrial processing in addition to, as the "metal-basis" indicates, an unknown amount of organic impurities. Given this, it is difficult to know whether grown copper thin-films via atomic layer deposition (ALD) would also suffer from the same problems, that is, what is a critical amount of carbon impurity to affect the growth?

1.2.1 Nucleation

Important both for fundamental studies of thin-film growth and technological innovation, understanding graphene nucleation would enable controlled growth of graphene domains to the desired size. This is important due to the scattering nature of graphene grain boundaries, formed from the coalescence of 2 or more grains, for electronic purposes. Naturally, to study this, one looks at what encourages and suppresses nucleation. A lot of work has centered on pre-treatments (prior to the introduction of a carbon precursor, i.e., prior to the growth phase) to suppress nucleation often with little to no mechanism put forth.

1.2.2 Large Area Grains

Inherently tied to nucleation is the size of graphene domains. This is because the nucleation density in an average growth is high enough that the coalescence of these domains is the limiting factor to the size of the individual domains. Therefore, a perfect understanding and control of nucleation would enable one, in theory, to grow a domain to the extent of the substrate.

1.2.3 Bilayers

Bi- and multi-layers on copper have always puzzled researchers. That a three-dimensional element could occur in a system seen to be two-dimensional, since the dehydrogenation of methane depended on the catalytic power of the substrate, was peculiar indeed. After all, upon completion of the first graphene layer, this would serve as a barrier and cap the copper from the incoming gas leaving no possibility for atomic carbon to eventually lie on the surface. A link between nucleation and bi-multilayers is a little less intuitive. However, due to our work in understanding the impact of carbon impurities in the bulk and surface processes there is evidence that both are related.

This thesis is divided into three parts: context, methods and results. The first is done through an introduction (chapter 1) and literature review (chapter 2). Methodology (chapter 3) establishes the physical setup bringing to attention what is unique in our understanding as is reflected through our customization (i.e., the purifiers) while the results, its understanding and elaboration are expounded in the model section (chapter 4), results (chapter 5) and the associated discussion (chapter 6) with a look to the possible future in perspectives (chapter 7) and finishing with an appendix consisting of the mathematics involved behind the model we present.

CHAPTER 2 LITERATURE REVIEW

In this section we first introduce the current understanding of substrate-carbon precursor interplay with a generalized introduction to graphene formation via CVD using methane as the carbon source. Next, we provide a more in-depth investigation and review of graphene formation starting from methane dehydrogenation on copper to active surface-bound carbon species and finally nucleation. Lastly, we present current thoughts and trends regarding the impact of oxygen prior to and during graphene growth touching upon its possible role in methane dehydrogenation, role in nucleation, ridding of surface-bound and bulk-bound carbon, large-area graphene as well as the formation of bi/multi-layers.

2.1 Graphene Growth via Chemical Vapor Deposition on Copper using CH_4/H_2

The first method used to isolate graphene was done via exfoliation of highly oriented pyrolytic graphite (HOPG) in 2004.[11] Since then, many techniques have been used to synthesize graphene: reduction of graphite oxide[23], high temperature annealing of silicon carbide (SiC) in UHV conditions[24] and CVD on metal substrates.[25] While all these methods can be viable depending on the application, none individually cover the range as well as CVD on metal does due to its unique combination of low cost, high through-put monolayer graphene with low defect and ease of transfer.

In principle, CVD growth of graphene is rather straightforward requiring only a carbon precursor, substrate and an elevated enough temperature for growth which is dependant upon both the precursor and the substrate. For example, on copper, temperatures as low as $300°C$ are possible when using benzene as the carbon precursor while $500°C$ has been reported with polymethyl-methacrylate (PMMA) and polystyrene as a carbon source.[26] Another group has reported an optimal growth temperature of $850°C$ for alcohols (ethanol, methanol and propanol) with $750°C$ as the lowest temperature, though with a much poorer quality.[20] By and large, methane is the preferred precursor for graphene with no discernible reason evident in the literature – perhaps owing more to historical reasons than anything else – with temperatures ranging from $950°C$ to $1050°C$.[14,27,28,29,30,31,32]

Graphene growth on Ir,[33] Ru,[34] Ni,[15] Pt,[35] Pd,[36] Co[37] and Cu have all been reported with varying levels of success. These transition metals follow two possible routes to graphene nucleation: one of carbon incorporation/dissolution into the bulk followed by segregation and/or precipitation to the surface (Fig. 2-1 (a)) or a purely surface-mediated nucleation (Fig. 2-1 (b)). For carbon to diffuse into the bulk a non-negligible carbon solubility (at synthesis temperature) is required, making this parameter the primary one in determining the nucleation mode. For Ir, Ru, Ni, Pt and Cu carbon solubilities of 0.041 at.%,[38] 0.34 at. %,[38] 0.6-0.9 at. %,[39,40] ~$(3.1 - 43)x10^{-4}$ at. %[41,42] and $(7.4 – 80)x10^{-4}$ at. %[39,43] are reported at $\sim 1000°C$, which serve to explain why the first 3 transition metals follow a bulk diffusion and segregation mode whereas copper is believed to be surface mediated with results being inconclusive in the case of platinum.[38]

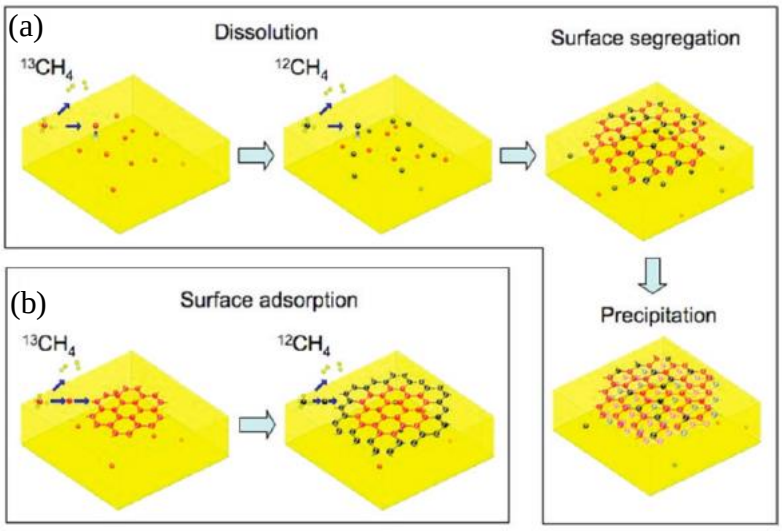

Figure 2-1 Different growth modes following a) dissolution, surface segregation and/or precipitation (e.g. Ni) and b) surface adsorption due to low carbon solubility (e.g. Cu). Reproduced with permission from ref. 40. American Chemical Society, copyright 2009.

As a direct consequence of copper's carbon solubility, it is easier to grow monolayer graphene on copper compared to most other substrates. As a result, copper has emerged as a substrate of choice for CVD graphene synthesis due to its availability, cost and growth mechanism. With a very low carbon solubility and a calculated mobility said to be a purely surface-based process,[44] copper plays a very different role compared to other transition metals. Ruoff et al.[40,45] demonstrated via Raman imaging the surface-mediated nature of graphene synthesis on copper by doing alternating pulses of $^{13}CH_4$ and $^{12}CH_4$. Intuitively, for a material where the bulk does not enter into the equation and the growth is limited to being surface-mediated, the expansion of these

2D islands will grow laterally from a point of nucleation either until the grain grows to the extent of the substrate or it coalescences with another graphene grain. On the other hand, if the carbon were to diffuse into the bulk then any sense of order (since there will be a sequential order to the carbon as one might relate tree rings to age) would be lost (Fig. 2-2 (c)). Therefore, in order to demonstrate this, Ruoff et al. used different isotopes of carbon in sequential order during the growth which showed a delineated phase difference in the case of copper (Fig. 2-2 (a,b)) and a loss of order in the case of nickel.

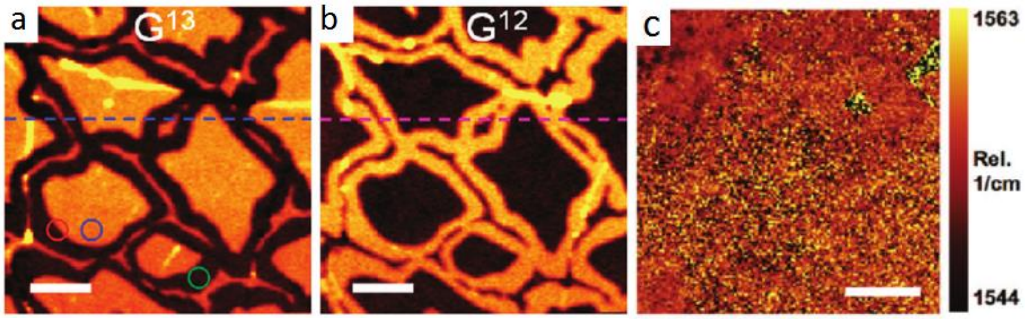

Figure 2-2 Raman G peaks for the different carbon isotopes demonstrating the nature of different growths modes on a & b) Copper and c) Nickel. The pulsed growths show the a) surface mediated growth on Copper using $^{13}CH_4$ followed by $^{12}CH_4$ and b) the dissolution of the carbon in nickel which then precipitates and/or segregates showing no clear delineation of the ^{13}C and ^{12}C phases. Reproduced with permission from ref. 40. American Chemical Society, copyright 2009.

The pathways from carbon precursor to adsorbed carbon is notoriously difficult to nail down due to the nature of intermediate species and their interaction with the substrate, resulting in most of the information related to this coming from simulations.[46] Loosely, the methane undergoes dehydrogenation catalyzed by the transition metal until carbon is left at the surface at which point, depending on the transition metal, it will either diffuse into the bulk or remain mobile on the surface. In this regard, not only is the catalyst important but the crystallographic orientation is as well, due to their differing catalytic power. For example, in the hypothesized first step of methane dehydrogenation ($CH_4 \rightarrow CH_3 + H$), Cu(111) and Cu(100) have approximately the same energy barrier but will then differ for the subsequent steps, with Cu(100) having a lower barrier than Cu(111).[46]

In addition to this left-over hydrogen from the methane dehydrogenation, molecular hydrogen is also added as a process gas during the graphene growth. Hydrogen's precise role during graphene synthesis has been the subject of much debate in the literature.[47,48,49] Hydrogen has been

thought to be a kinetic inhibitor by blocking available Cu sites,[50] an etchant[51] as well as a cocatalyst "in the formation of active surface-bound carbon species (C_yH_x)".[51] Contributing in a significant way to this discussion, Choubak *et al* showed that not only did hydrogen not etch when using purified ultra-high purity (UHP) hydrogen[21] but, rather, that hydrogen served to protect and counter-balance the etching due to oxidizing impurities found in the gases.[52]

2.2 **Nucleation**

This literature review will be divided into two parts: firstly, a brief but more detailed introduction to nucleation of graphene on copper *via* CVD to not only provide a broad view of the domain but to serve as a back-drop for the second part, mainly, the impact of oxygen on graphene nucleation. To elaborate: that carbon is burned by oxygen at $1000°C$ is less than surprising, however, as hinted upon in the previous literature review, if it's true that the carbon solubility of copper is elevated *enough* to have an impact on nucleation, then in what way can oxygen be used to impact said nucleation. It is this kind of oxygen-copper-carbon interaction which will be focused upon in this review but also throughout the thesis.

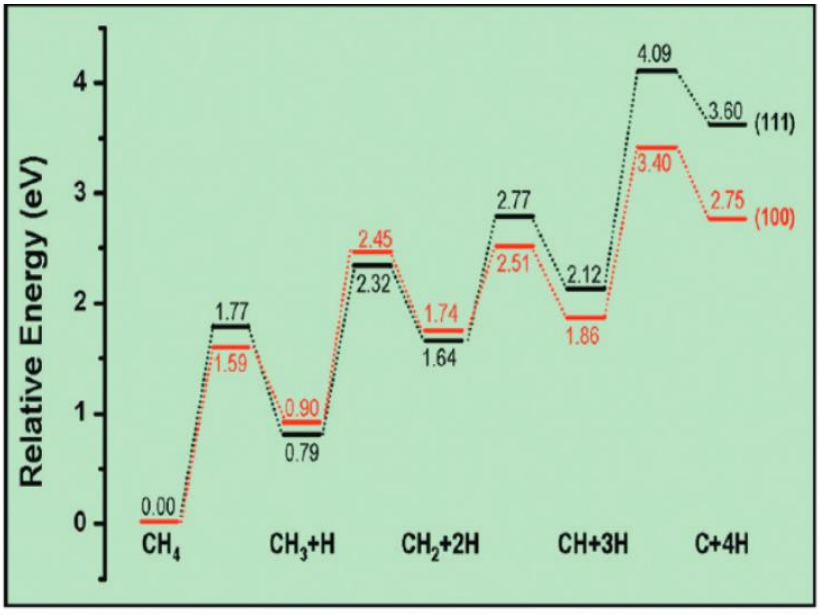

Figure 2-3 Energy of disassociation as a function of dehydrogenation steps for CH_4 relative to adsorbed CH_4 on Cu(111) and Cu(100). Reproduced with permission from ref. 53. American Chemical Society, copyright 2011.

There are three basic phases to graphene nucleation on copper: 1) the decomposition of hydrocarbon on the catalytic surface with the subsequent formation of active carbon species; 2) the nucleation of graphene *via* aggregation (due to a saturation threshold being met) of said active carbon species and 3) lateral expansion of graphene nucleation *via* carbon adatom diffusion and attachment. Despite each methane dehydrogenation step being endothermic and therefore unfavorable, with the final $C + 4H$ product modeled as being 3.60

eV and 2.75 eV higher than the adsorbed CH_4 on Cu(111) and Cu(100), respectively (Fig. 2-3),[53] this reaction still proceeds due to the elevated growth temperatures at or above $1000°C$. Some[54] within the literature also propose a mechanism by which the inclusion of solid C at the surface shifts the gas-phase equilibrium from one where C_xH_y radicals are non-negligible to negligible. That is, within their density functional theory (DFT) calculations, upon the introduction of solid C on their substrate surface, almost all the CH_4 became converted to solid carbon and hydrogen, leading to a significantly reduced presence of CH_3, C_2H_2, C_2H_6 (Fig. 2-4), meaning that dehydrogenation and graphene nucleation happens more efficiently if solid-phase carbon is present at the surface (this prospect becomes particularly interesting given the objective of this thesis. Within their calculations the solid C introduced would simply be a cascading effect from the initial graphene nucleation to further shift the methane dehydrogenation in the direction of solid carbon $CH_4 \rightarrow C + 4H$, however, conceivably this carbon could be due to carbonaceous impurities from within the bulk working its way to the surface, as we suggest in our model).

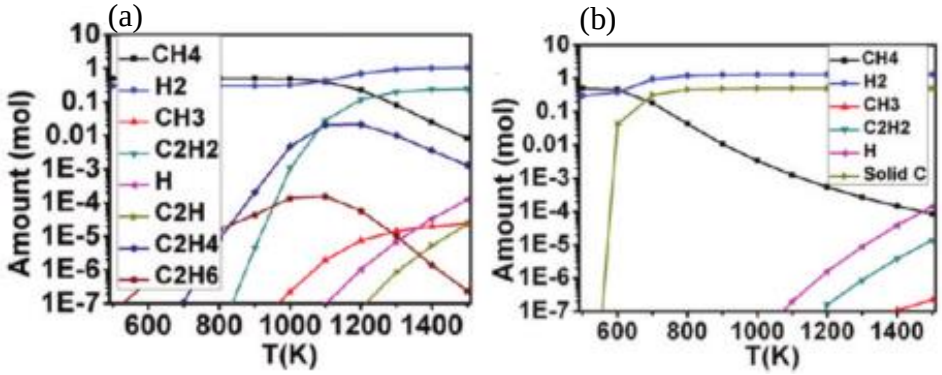

Figure 2-4 Mole fraction (with an initial $H_2:CH_4 = 3:5$) on Cu in (a) gas-phase equilibrium from 500K to 1500K of methane pyrolysis) (b) gas-phase and solid-carbon-phase equilibrium with a total pressure of 20 Torr H/C=26:5. Reproduced with permission from ref. 54. American Chemical Society, copyright 2012.

By and large, most information concerning the active carbon species are theoretical due to the nature of the problem. Intuitively, one of the factors that will determine the type of carbon mono/di-mer and radical (C_xH_y) that will be involved in growth and nucleation is the strength of the metal-carbon interaction. For example, as was calculated by DFT, the subsurface of Cu(111) has the largest binding energy at 5.39 eV[55] for the carbon monomer, with similar results reported elsewhere for different copper facets.[56] That the subsurface is the preferred site is due to the coordination number (defined as the nearest neighbors, i.e., 2 for a string of carbon, 3 for graphene,

etc.) being more elevated than at the surface (from 4 to 3) reducing the adsorption energy. However, it is important to note that this is a function of temperature such that if we reduce the growth temperature to 1000K ($730°C$) the population of CH radical is greater than the C monomer (Fig. 2-5 (d)).

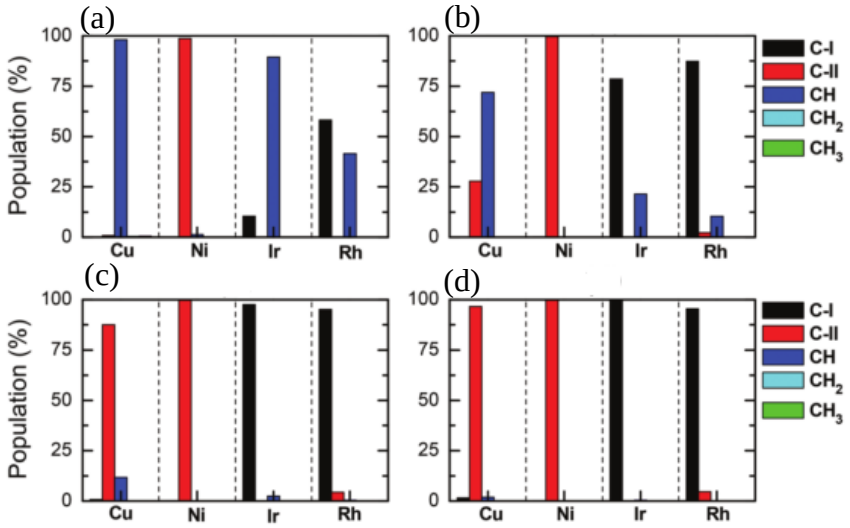

Figure 2-5 Population ratios of various CH_x species and carbon monomers (C-I and C-II for surface and subsurface carbon monomers, respectively,) on Cu(111), Ni(111), Ir(111), Rh(111) at (a) 800K, (b) 1000 K, (c) 1200 K, (d) 1400K. Reproduced with permission from ref. 55. The Royal Society of Chemistry, copyright 2015.

The rate at which graphene nucleates will dictate the concentration of nuclei which, in turn, will affect the possible domain size produced limited by eventual coalescence (i.e., the lower the concentration of nuclei the larger the grains will grow until coalescence). To demystify the structure of these nuclei structures Wesep *et al*,[57] using first-principles calculations within density functional theory, calculated the ground state of carbon clusters C_N from $N = 3 \ldots .13$ where they found that, due to the strength of the C-C bond relative to C-Cu, 1D linear structures (Fig. 2-6 (c)) were more stable than compact 2D structures (Fig. 2-6 (b)) due to the unfavored highly-bent divalent carbon atoms. As can be seen from figure 2-6 (a), while the formation energy over the whole number of atoms calculated is lower for linear structures as opposed to a compact one, the authors also admit that in a real-world setting at the typically high temperatures used during graphene growths, both structures could co-exist. The meta-stability of a hexagonal ring (6C), the smallest meta-stable island found, was calculated to be 0.66 eV − an energy barrier that could be easily overcome at standard growth temperatures. However, once 10 carbon atoms come together to form two closed rings, 2 bonds would need to be broken which is less favorable with a similar

argument being extended to 13C, suggesting that these 2D chains are relatively short-lived with typical cluster sizes between 10-13 carbon atoms.

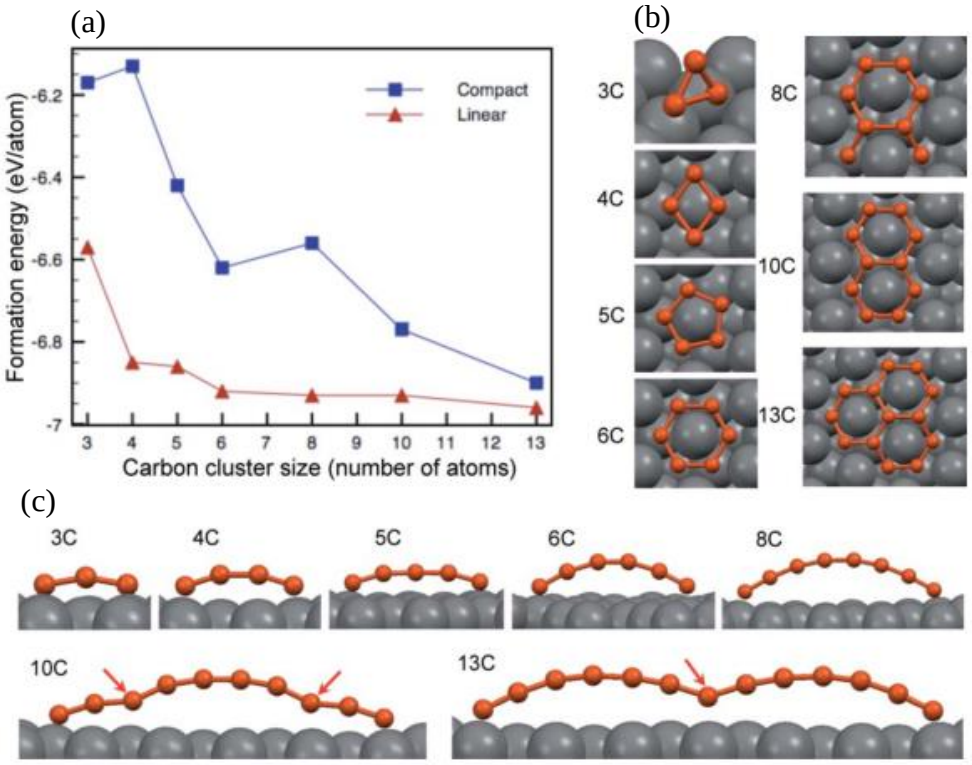

Figure 2-6 (a) Formation energy of linear and compact structures per carbon atom. (b) 2D compact structures for $N_C = 3, \ldots, 13$ on Cu(111). (c) Linear 1D structure for $N_C = 3, \ldots, 13$. Reproduced with permission from ref. 57. AIP Publishing Group, copyright 2011.

2.3 Oxygen and Graphene Growth

Whereas oxygen was previously shown to inhibit growth,[21] recent trends have leaned towards adding oxygen to the system to better investigate its impact on graphene growth, as will be shown in this section.

2.3.1 Dehydrogenation

On a more macro scale, oxygen has been noted both as a nucleation/growth inhibitor and enhancer.[54,55,56,57] The adsorption energy of various species, $CH_4, CH_3, CH_2, CH, C, H, O,$ and OH, were calculated by DFT on transition metal surfaces[58,59] with Cu(111) being relevant to our study. Here it was found that in cases where the C atom has unsaturated bonds ($CH_x; x = 0, \ldots, 3$), carbon-metal ($C - M$) bonds are formed between the carbon sp^3 and the metal d-states[58] with the energy

of adsorption increasing with decreasing number of H atoms. However, when an oxygen atom is present on the surface, the $O-M$ bond competes with the CH_x-M bond, altering the charge distribution. Through this, a charge transfer occurs both from the copper and the oxygen atoms to the carbon atoms as opposed to solely the Cu atom, which increases the adsorption energy of the carbon atom on a pure Cu(111) surface by 0.99 eV (7.04 eV compared to 6.05 eV).[60] Oxygen was also shown to increase the adsorption energy of CH_4 meaning that adsorbed oxygen on copper could play a role in every step of methane dehydrogenation. In a relatively old study,[58] this result was demonstrated when CH_4 was found to react with oxygen-chemisorbed Cu(100) at $430°C$ whereas it would only react with clean Cu(100) at temperatures above $530°C$. This result was also corroborated by DFT calculations[61] where it was found that the first step of methane dehydrogenation was initially 1.57 eV which went down to 0.62 eV with the presence of oxygen.

2.3.2 **Nucleation**

In the same way that copper surface irregularities (steps[62,63], impurities[64,65] and grain boundaries[62,66]) have long been thought to play a role in graphene nucleation, oxygen-rich copper

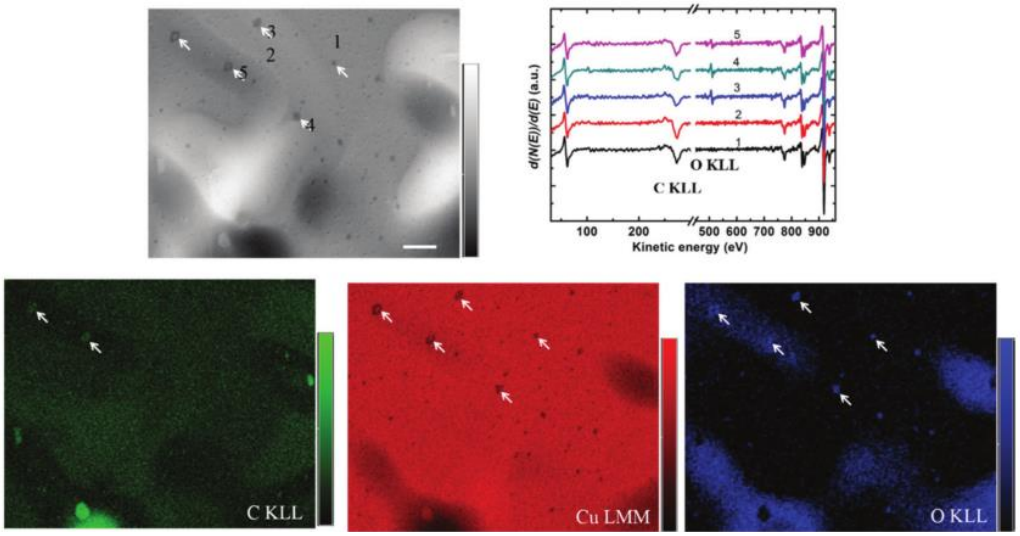

Figure 2-7 (a) SEM micrograph showing AES acquisition sites. (b) Differential AES acquired from sites "1-5" in (a). (c-e) C KLL, Cu LMM, O KLL Auger electron maps. The graphene nuclei appear at the sites with a strong oxygen signal. Reproduced with permission from ref. 60. The Royal Society of Chemistry, copyright 2015.

sites are also thought to be able to initiate nucleation.[60] This was demonstrated by observing that the Auger electron spectra oxygen KLL (Fig. 2-7 (e)) signal at the presumed nucleation sites

(interpreted as the locations with an elevated intensity in the C KLL signal (Fig. 2-7 (c))) were much stronger than at the bare Cu surfaces (Fig. 2-7 (d)). On the other hand, others hypothesize

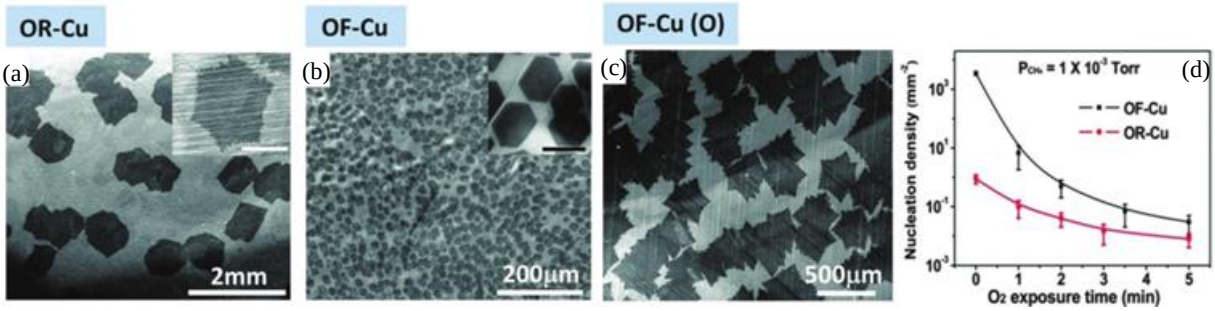

Figure 2-8 (a-c) SEM images of graphene domains on OR-Cu, OF-Cu and OF-Cu(O), respectively. Insets in (a) and (b) show magnified images with scale bar of 500 μm and 20 μm, respectively. (d) Graphene nucleation density as a function of O_2 explosure time for OF-Cu (red) and OR-Cu (black). Reproduced with permission from ref. 67. American Association for the Advancement of Science, copyright 2013.

these sites would participate in the surface reaction preferentially due to their dangling bonds. This increased adsorption energy would make it much more likely that these sites would be passivated and lose their ability to assist in hydrocarbon capture (and subsequent decomposition), resulting in a decreased nucleation density when treating the surface at high temperatures before the hydrocarbon is introduced.[67] This idea was explored by using oxygen-rich (OR) and oxygen-free (OF) copper. It was found that not only was the nucleation density of OR-Cu much lower than that of OF-Cu but annealing oxygen-free copper in oxygen (OF-Cu (O)) diminished the nucleation density to that of OR-Cu as a function of O_2 exposure time (Fig. 2-8 (d)).

2.3.2.1 Surface Adsorbed Carbon

Many authors[68,69,70,71] attribute the impact of oxygen on nucleation to purely surface-oxygen phenomena. Chen *et al.*[68], using ethanol as their carbon precursor, reported 5mm wide graphene domains, which they attribute to their ultra-low partial pressure of ethanol ($4x10^{-4}$ Torr) and a copper pre-oxidizing step (done in ambient air). Solely using a low flow of ethanol, a nucleation density of $8\,mm^{-2}$ was further reduced to $0.1\,mm^{-2}$ by pre-oxidizing the copper substrate at $250°C$ for 90 minutes yielding 5 mm large graphene domains. They surmise that the oxygen-rich copper foil is a result of the copper-oxide, in the form of CuO and Cu_2O, diffusing into the bulk which, in turn, would eventually play a role in Cu surface passivation thereby reducing the nucleation density. It should be noted that, regardless of the oxygen pressure, a Cu_2O oxide would not be formed at $250°C$ according to the phase diagram.[72] Instead of pre-oxidizing their copper,

Magnuson *et al.*[69] opted for OR-Cu and attributed a diminution in nucleation density to the oxygen released from the copper-oxide reduction, interacting with adventitious surface carbon, which they demonstrated as being persistently present despite nitric acid, acetic acid or acetone cleaning of the copper substrate. In addition to nucleation experiments, they also had a gas-analyzer at the furnace output to measure the partial pressure of $CO_2, CO,$ and O_2, which show the interaction between O_2 from oxidized OF-Cu and quantity of surface carbon residue (Fig. 2-9).

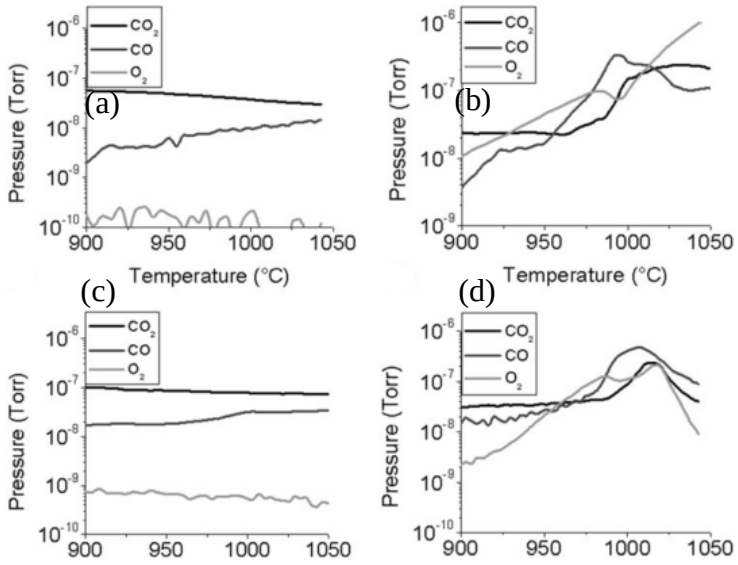

Figure 2-9 Oxygen, carbon monoxide and carbon dioxide partial pressures in CVD system vs furnace temperature on initial heating of (a) CVD chamber and sample holder, (b) oxidized OF high conductivity (HC) copper, (c) OFHC-Cu, and (d) 99.8% copper. The background from (a) was subtracted for all proceeding measurements. Reproduced with permission from ref. 69. The Cambridge University Press, copyright 2014.

Along the same vein, Miseikis *et al.*[70] realized that any kind of oxide (pre-oxidized or as-received) would be lost if one proceeded with a typical graphene growth using hydrogen as this would act as a reducing agent. Instead, using Argon during the anneal to maintain the copper oxide until initiation of graphene growth, a reduction in graphene nucleation with subsequent enlarged graphene domains was demonstrated, owed largely to the preserved oxide, though no mechanism was offered. Lastly, Pang *et al.*[71] demonstrated through a series of experiments that the small graphene islands that appear in their SEM micrographs originate prior to the introduction of the methane (and thus, prior to the growth phase) as deduced from the complete absence of these when annealed in an oxygen environment, suggesting they have organic surface contaminants as their nucleation source.

2.3.2.2 Carbon in Bulk Copper

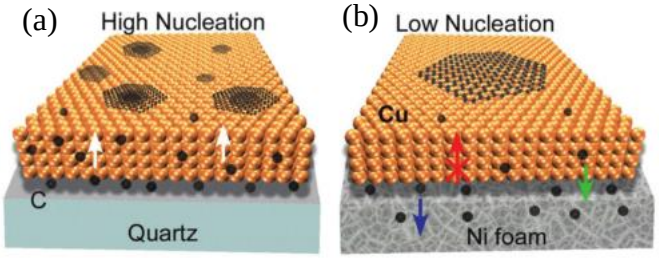

Figure 2-10 Proposed model illustrating the impact of (a) bulk carbon on graphene nucleation and (b) a nickel foam support as a carbon getter on nucleation. Reproduced with permission from ref. 73. John Wiley and Sons, copyright 2017.

While some have suggested that surface organic contaminants play a role in graphene nucleation, there has been important work done on identifying these contaminants in the bulk and understanding their role in graphene growth and nucleation.[24,73,74] A unique approach has been taken to investigate the "influence of the support substrate on the kinetics of graphene growth" whereby a nickel foam was used as a backside support of their copper foil to act as a carbon getter (Fig. 2-10 (b)) due to its high carbon solubility.[73] They demonstrated this by using 3 different kind of supports: Cu/quartz (Fig. 2-10 (a)), Cu/quartz(Cu) (quartz coated with copper) and Cu/Ni followed by graphene growth. The phenomena they focused on were the growth of graphene on the backside, the formation of multilayers and the growth of large-area graphene domains. Interestingly, they observed a close correlation between topside and backside coverage percentage, suggesting that methane first finds its way in the microgap between the copper and the support substrate, undergoes dehydrogenation as expected resulting in carbon at the surface from where it diffuses into the bulk and works it way to the top surface of the copper. Eventually, a threshold carbon concentration is reached and graphene nucleation is initiated on the backside which, once the layer completed, passivates the surface resulting in no carbon being able to diffuse

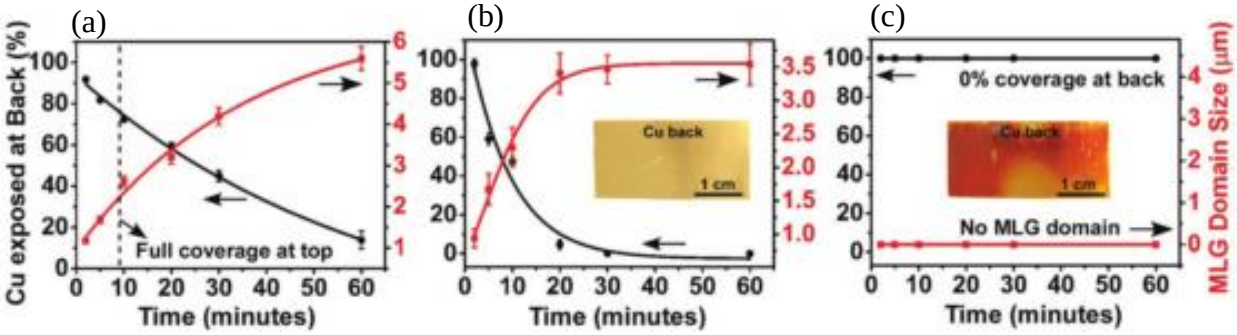

Figure 2-11 Correlation between backside coverage and topside multilayers on (a) Cu/Quartz (b) Cu/Quartz(Cu)and (c) Cu/Ni. Reproduced with permission from ref. 73. John Wiley and Sons, copyright 2017.

through the bulk to the top surface, terminating top surface multilayer growth (Fig. 2-11). Despite

the presence of this microgap, no multilayer graphene was found on the copper with a nickel backing suggesting that the lack of carbon species available to cause nucleation was due to the nickel "gettering" action. However, that nickel has a higher carbon solubility than copper does not explain why carbon would wholly and solely interact with the nickel. Leaning on DFT calculations, they demonstrate that nickel provides preferential binding sites for carbon, offering a thermodynamic driving force for carbon to diffuse toward the nickel instead of the copper. Nevertheless, they demonstrate that carbon can diffuse through the copper foil and can initiate nucleation, in multilayer form or otherwise.

In a similar vein, but focusing on pre-treatments to rid the deleterious carbon impurities, recent work has reported a diminution in graphene nucleation density in connection to oxidizing pre-treatments.[27,74] The second of these studies attempted to tease apart the impact of oxygen diffusion through the copper bulk and any subsequent chemical effects from surface roughness.[74] To do this they oxidized the backside (or BO for backside oxidization) of the copper foil (i.e., the side which resides on the quartz substrate) by floating it over a 30% H_2O_2 solution at $100°C$ for times between 0 and 300 s (with 300s yielding approximately a 70 nm thick oxide) and annealing in an Argon environment in order to maintain the oxide which would not occur in a typical H_2 environment. What was found *via* time-of-flight secondary ion mass spectrometry (TOF-SIMS) was that a reduced C_2^- intensity was observed for the BO + Ar samples, compared to Ar:H_2 and Ar annealing (Fig. 2-12 (a)), as well as a reduction in nucleation density by 4 orders of magnitude (Fig. 2-12 (b)). They propose a mechanism by which the oxide decomposes into its constituent parts (Cu and O), diffuses within the bulk to act as a carbon scavenger bringing said carbon to the surface, which then possibly leaves in the form of CO_x (Fig. 2-12 (c)). They suggest two possible avenues by which the carbon could segregate to the bulk: the areas of high carbon concentration may correspond to graphitic or amorphous carbon which would naturally diffuse at a much slower rate than atomic carbon and could be ingrained during the manufacturing cold rolling process, or from hydrocarbon dissociation at the catalytic surface before a supersaturation occurs, initiating nucleation. In a similar study, Kraus *et al.*[27] suggest the carbon content within standard 99.8% polycrystalline copper foil used for graphene growth could be anywhere between 40-240 monolayers (ML) of carbon. While carefully maintaining the oxygen pressure to below that which would form an oxide ($1x10^{-5}mbar$) to avoid morphologically driven effects on the graphene nucleation, a reduction in the *ex-situ* X-ray photoemission spectrometer (XPS) C 1s (scaled in

relation to the Cu 3s peak) signal was observed, resulting in 15% of a ML of carbon remaining after 6 hours of oxygen exposure. Leaning on other work reporting bulk dissolved carbon to be between 5 and 200 ppm[43] (which yields approximately 1-28 ML given the dimensions of the copper foil being used in this case), it becomes clear that the amount of carbon exceeds what should normally be found under equilibrium conditions, due to which, they suggest, the excess carbon may come from the copper cold-rolling process. Once rid of this due to the backside oxidization treatment, a density of 7 flakes$/mm^2$ with graphene domains of diameter >500 μm were reported using 5 mTorr of CH_4.

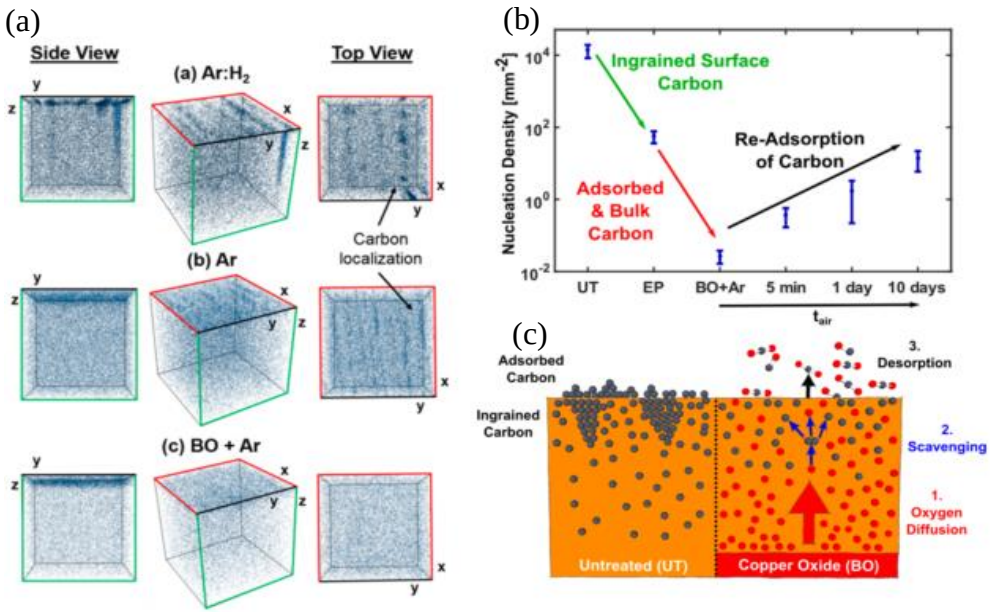

Figure 2-12 (a) TOF-SIMS of the 3 annealing environments with different views of the copper bulk and carbon impurities found within. (b) Nucleation density as a function of pre-treatments (UT = untreated, EP = electropolishing which both constitute surface related carbon reduction methods) and (c) Proposed model for 1. oxygen diffusing from backside copper oxide to 2. bulk carbon scavenger and lastly 3. desorption of carbon species. Reproduced with permission from ref. 74. The Royal Society of Chemistry, copyright 2016.

2.4 **Bi/Multi-layers**

Since its discovery, bilayer graphene has attracted attention both for its technological applications as well as the fundamental answers an understanding of its growth mechanism could provide. An ability to control the formation of bilayers could enable the exploitation of its non-zero bandgap (with an applied vertical electric field) as well as help assure a better control over

monolayer graphene growth since an understanding of bi- and multilayer mechanisms should lead to ways in which these could be suppressed during regular monolayer growths.

Unsurprisingly, there exists 2 growth mechanisms for graphene bilayers, mainly, wedding cake/on-top layer (Fig. 2-14 (a)) and inverted wedding cake/under layer (Fig. 2-14 (b)). What is surprising, however, is that even on a transition metal like copper, whose growth mode is seen to be wholly surface mediated, these two competing theories are used to explain the presence of bilayers. The arguments follow as an extension from the understanding of monolayer growth mechanisms: since the catalytic surface is necessary for the dehydrogenation of methane it should follow that the bilayers will form under the first layer.[75,76] On the other hand, evidence has been found to support the opposing view,[77,78] which would be more in line with traditional crystal growth in which new layers are grown on top of pre-existing ones. With this lack of consensus within the literature, the search and explanation for the elusive mechanism for bilayer growth carries on.

Four different mechanisms were identified that could lead to an inverted wedding cake growth mechanism: precipitation from the bulk – said to be not suitable for those transition metals with low carbon solubility like Cu[79] (Fig. 2-14 (b)I); by carbon adatom surface diffusion from the bare catalytic surface to under the first layer said to be possible if the edges of the graphene islands are passivated, e.g., by hydrogen[79] (Fig. 2-14 (b)II); by penetrating the first layer *via* a carbon exchange process[80] (14(b)III) and lastly through a impurity-induced defect in the graphene monolayer.[81]

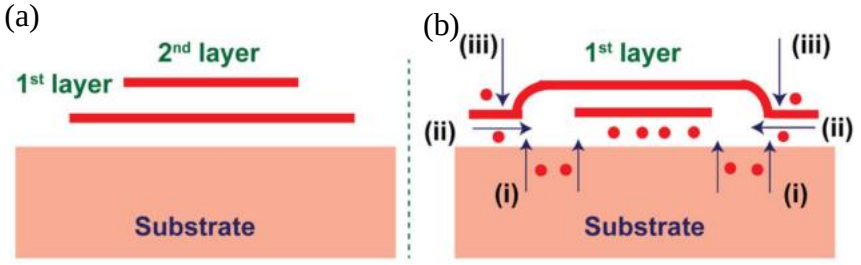

Figure 2-10 Two proposed models for graphene bilayers (a) Wedding cake and (b) Inverted wedding cake. Reproduced with permission from ref. 79. IOP Publishing, copyright 2018.

As with most other aspects concerning the impact of oxygen on graphene growth, its role in the growth or inhibition of graphene bi/multi-layers is not agreed upon. Hao *et al*[77], using a copper pocket growth (Fig. 2-15 (a)), made use of OF-Cu and OR-Cu to demonstrate that the dissolution of carbon atoms into copper necessitates the presence of oxygen to be possible. By

conducting the same growth on these two samples, they observed that the exterior of the OR-Cu had bilayers which was not the case for the exterior of the OF-Cu. Therefore, they surmise, oxygen opens the kinetic pathway to bilayer growth by decreasing the barrier for CH_x attachment, suggesting that the OF-Cu acts as a sort of barrier for CH_x. Others suggest the oxygen can intercalate itself between the graphene and copper (either in oxygen form or copper oxide, yielding the same result), allowing for carbon adatoms to diffuse under and form bilayers.[82]

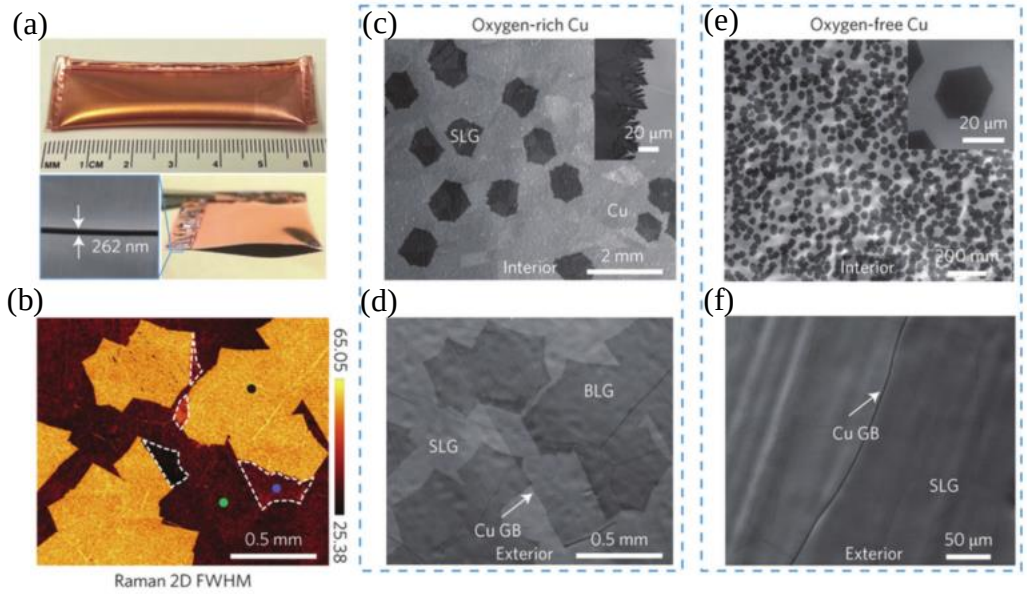

Figure 2-11 (a) Image of copper pocket with edges crimped. (b) Raman map of 2D peak FWHM. OR-Cu (c) interior and (d) exterior. OF-Cu (e) Interior and (f) exterior. Reproduced with permission from ref. 77. Nature Publishing Group, copyright 2016.

2.5 **Gas-Phase Oxygen Impurities**

Thus far the bulk of the discussion has focused on the impact of oxygen impurities along the different phases of graphene synthesis (i.e., dehydrogenation, nucleation, etc.) mainly within the context of carbon purification. However, other ways exist by which oxygen can be present within the system with much larger implications than the scientific community gives it credit for. Certainly, most research groups take exceptional care, whether done in APCVD or LPCVD, in being able to control the gases present within the chamber such that avoiding leaks is self-evident. Unfortunately, this does not take into account oxygen impurities present within the process gases themselves, which are often thought to be too low – at the ppm level – to impact graphene synthesis.

To demonstrate the impact of oxygen impurities within gas-feedstock, Choubak *et al.*[83] installed a DEOXO ($O_2 < ppb$) purifier on the hydrogen line as well as a by-pass to avoid said purifier. Using completed graphene on copper, annealing experiments at $825°C$ were done under three conditions: 1) under vacuum, 2) under 500 mTorr of as-received UHP 99.999% hydrogen ($O_2 < 1ppm$) using the by-pass and 3) under 500 mTorr of UHP hydrogen filtered by the DEOXO purifier. The results, seen in Fig. 2-12, show that only the annealing done under unpurified hydrogen showed etching in the graphene film.

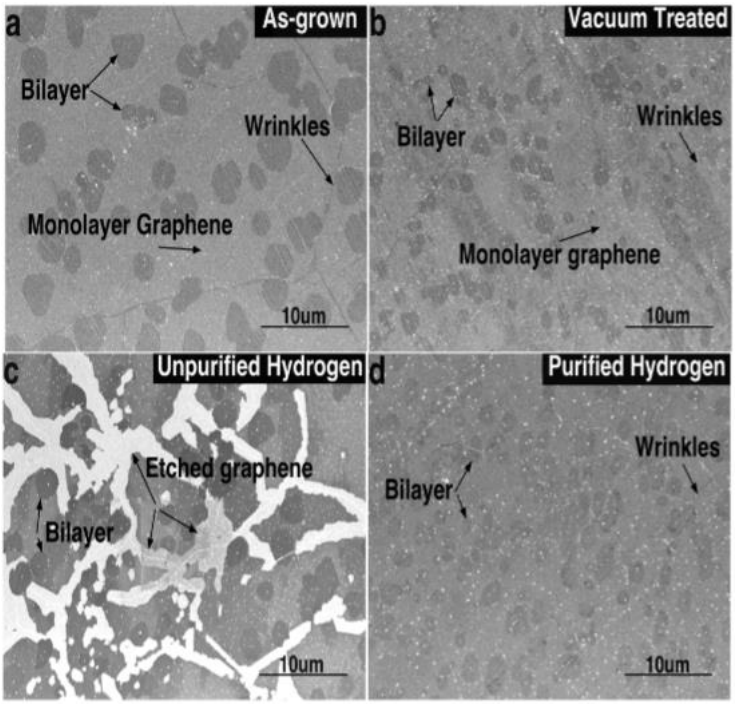

Figure 2-12 SEM micrographs showing a) as-grown graphene on copper used as the basis, b) vacuum treated graphene, c) annealed graphene by-passing the DEOXO purifier and d) annealed graphene using the DEOXO purifier. Reproduced with permission from 84. American Chemical Society, copyright 2013.

In a similar vein, Choubak *et al.*[84] explored the role of hydrogen and oxidizing impurities during graphene synthesis. By carefully selecting the phase – annealing, growth and cooling phase – during which gases would be turned on and off, coupled with the usage of purified and unpurified methane, a matrix was formed clarifying and decoupling the roles of hydrogen from oxidizing impurities and the role of purification of process gases in general (Fig. 2-13). More specifically, it was found that hydrogen in general was not required when using purified methane. Additionally, while many within the scientific community believed, and continue to believe, that hydrogen can

act as an etchant[85] from the reaction $2H_2 + C \overset{Cu}{\leftrightarrow} CH_4$, this study showed that purified UHP hydrogen does not etch. Both of these findings were attained by reducing oxidizing impurities from the process gases by use of a purifier from ppm to ppb levels. Interestingly, it was also found that graphene grown in these high purity environments had a higher bi- and multi- layer coverage, something accounted for by our model proposed in Chapter 4.

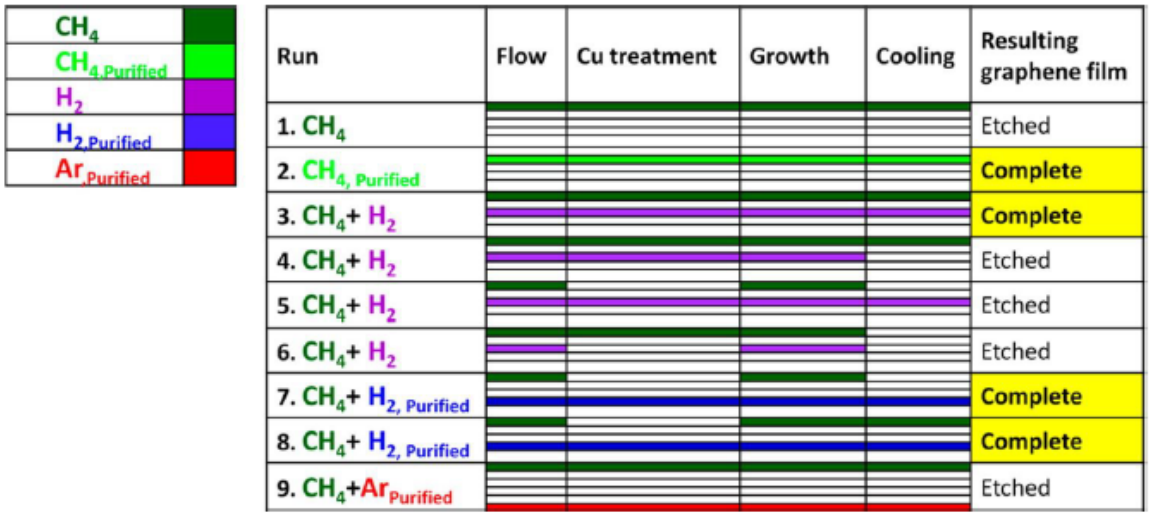

Figure 2-13 Growth experiments conducted. Filled lines indicate the gas mixture used in each experiment with the resulting graphene film as etched or completed. Reproduced with permission from 85. American Chemical Society, copyright 2014.

This chapter gave a general introduction to the details of methane dehydrogenation and the resulting active carbon species, serving as a backdrop to the impact of oxygen on nucleation. Widely varying opinions and results were presented relating the impact of oxygen on nucleation from being a nucleation promoter to it exclusively playing a role at the surface and lastly, as a carbon scavenger within the bulk. Oxygen as an impurity was detailed in more depth which demonstrated that without proper care of purifying conditions, this could make its way into graphene growth processes and serve as a growth inhibitor. Ideas related to carbon's ability to diffuse through the bulk were noted as well as a general overview of large graphene grains, which seem to be inextricably tied to low carbon-precursor pressure and a reduced nucleation. It's the hope of the author that this review section was clear in its confusion; that no consistent thought has really emerged is a result of the research area being at the cutting edge of graphene growth – quickly evolving with no ideas being cemented as "truths" quite yet.

CHAPTER 3 TECHNIQUES AND METHODS

In this chapter we describe in greater detail the graphene synthesis process used to produce the graphene used in this thesis as well as the setup and all it entails including gas lines, CVD reactor, pumps and purifiers. Next, we go over the characterisation methods used to study the graphene and finish with the image analysis techniques.

3.1 Chemical Vapor Deposition Reactor

Here we present the method used to grow graphene on copper using methane as carbon precursor and hydrogen as gas carrier at low pressures. This method has demonstrated monolayer graphene with $\sim 5\%$ bilayers[18] and needs a chamber able to reach high temperatures ($1000°C$), gas feedstock lines to bring the gas into the chamber and pumps to reach and maintain the desired pressure.

3.1.1 Reactor

The reactor itself consists of a 4' quartz tube, for its resilience to high temperatures, joined by glass-to-flange joints at both ends. Given that these are constituted of a glass-to-quartz gradient, they must remain outside of the reactors hot-zone, a Lindberg oven enabling us to attain the desired temperature of $1000°C$. The flanges themselves are KF25 flanges, which are limited in temperature up to $180°C$ and pressures down to $\sim 10^{-8}$ Torr due to the inherent limitations of the elastomeric o-ring.[86] These flanges, at one end, are connected to the gas feedstock lines and on the other the pumping system. The gas side consists of UHP gases, mainly methane, hydrogen and oxygen, which are all connected to their own MassFlow Controller (MFC), to a computer with the ability to control the gas flow in standard cubic centimeter per minute (sccm), and purifiers. Lastly, the gas lines, before the gas is introduced into the quartz tube, converge to one line so that the gas mixture is homogeneous. At the other end of the reactor is the pumping system which consists of a diffusion pump backed by a mechanical oil pump. The latter enables us to reach the appropriate pressure regime ($\sim 10^{-3}$ Torr) for the diffusion pump, which allows us to reach pressures of 10^{-9} Torr. Additionally, to give us another dimension of control over the pressure there are 2 bypasses which consist of lines connected to the diffusion pump but of smaller radius as to constrict the flow.

3.1.2 **Gas and Purifiers**

Three gases in total are used for our graphene growths. Hydrogen (Praxair, UHP, $O_2 < 1ppm$), Methane (Praxair, UHP, $O_2 < 15ppm$) and Oxygen (Praxair, Research grade 99.999%).

As to assure a minimum amount of oxygen impurities in our gas feedstock for reasons mentioned in Chapter 2, each line (except for oxygen) is equipped with its own purifier:

- Hydrogen: A DEOXO^{TM} purifier is used to catalyze an oxygen-hydrogen reaction to give off water. As there is little oxygen compared to hydrogen this does not affect the H_2 pressure. The purifier is composed of palladium beads through which the hydrogen must pass and results in an oxygen level $< 1ppb$.
- Methane: SAES Pure gas Inc. purifier based on catalytic action of nickel is used, however, no further information is available due to the proprietary nature of these purifiers. This reduces the oxygen content in the gas to $< 1ppb$.

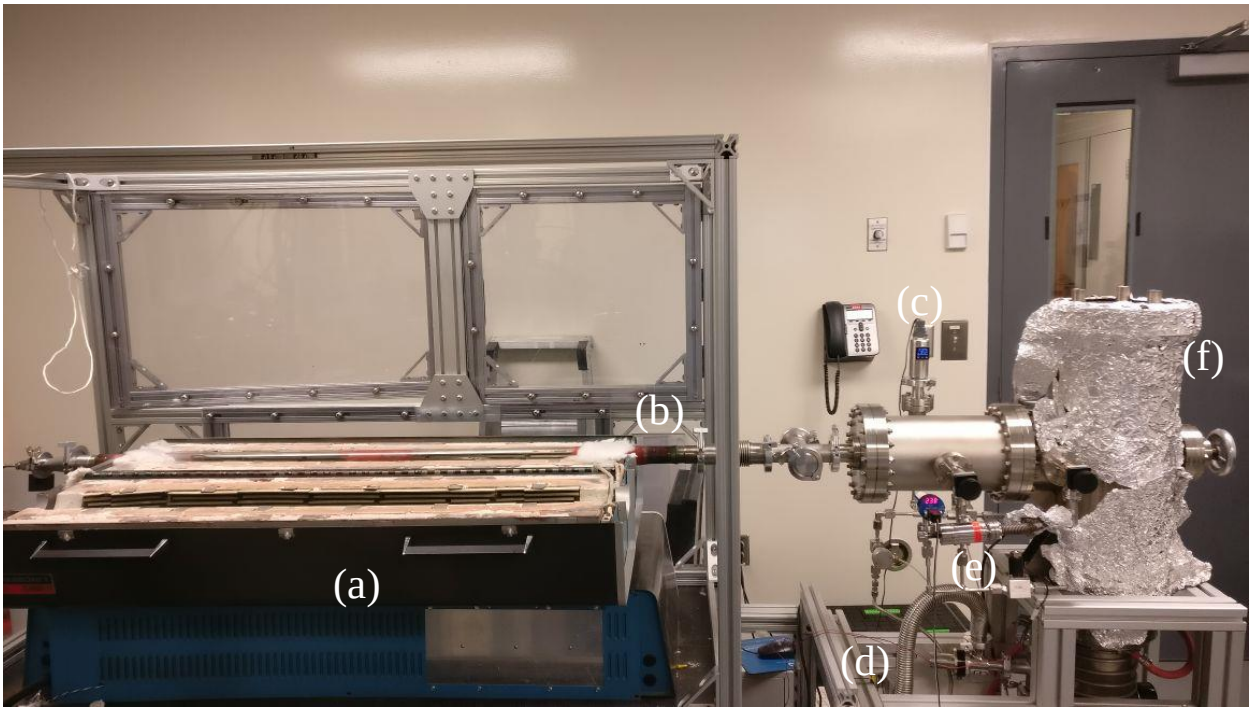

Figure 3-1 Image displaying the reactor and pumping setup. (a) Oven (b) Quartz tube (c) full-range gauge (d) Primary pump (e) by-pass (f) diffusion pump.

Despite the chemically rich environment present in the chamber due to all the gases introduced (CH_4, H_2, low levels of O_2) gas-phase reactions aren't expected to happen with methane being one

of the most thermally stable hydrocarbons, undergoing pyrolysis into acetylene at $\sim 1230°C$ and into ethylene at $1300°C$.[87]

3.2 Graphene Growth

In this section we go over the details regarding graphene synthesis from substrate preparation, annealing and pre-treatment to growth and lastly cooldown.

3.2.1 Substrate Preparation

The first step necessary in assuring consistent graphene synthesis is a cleaning step of our copper foil (*Alfa Aesar* 13382, 99.8% purity, 0.025 mm thickness). The cleaning proceeds in 3 steps:

- 10 minutes in a 1M solution of acetic acid at $60°C$;
- 10 minutes in acetone at $60°C$;
- 10 minutes in IPA at room temperature;

With these 3 steps completed, the copper oxide[88] and any kind of oil accrued through the manufacturing/processing are removed. The $1\ \text{inch}\ x\ 1\ \text{inch}$ foil is then placed on a quartz slide and loaded into the reactor.

3.2.2 Pre-Growth

There are 3 main phases before being able to start the graphene synthesis: the evacuation of the tube and insertion of H_2 processing gas, the temperature ramp-up and lastly the anneal.

From atmospheric pressure, the quartz tube is pumped down first with a mechanical pump until a molecular regime is reached, $\sim 10^{-3}$ Torr, followed by the diffusion pump which can push the pressure beyond the full-range gauge, $1.2x10^{-8}$ Torr, in approximately 30 minutes. Next, we introduce the processing gas that will be present during the temperature ramp up, H_2, to a pressure of $5x10^{-2}$ Torr. Once the hydrogen is stable we set the temperature to $1000°C$. Once 50 minutes have passed, $1000°C$ is reached and we can start the annealing phase as explained in greater detail in the results section. The gas is composed of hydrogen and oxygen phases varying in time depending on the experiment with the shortest anneal being 30 minutes.

3.2.3 Growth

Before proceeding to the growth, a diverting valve is used to deviate the hydrogen and methane to another pump to let the gases stabilize. Once stable, the valve is closed with the one to the main chamber opened and at this moment the growth timer is started. Once the desired growth is done the methane is cut with the hydrogen gas still present. Once the pre-methane hydrogen pressure is reached the heating is stopped and the oven is opened. The hydrogen valve is closed once $350°C$ is reached.

3.3 Characterization

The 2 characterization techniques used to assess the graphene are Scanning Electron Microscope (SEM) and Raman spectroscopy.

3.3.1 Scanning Electron Microscopy

As its name suggests, a scanning electron microscope functions by focusing a high energy electron beam to a fine point which rasters across the surface of a sample. The main beam interacts with matter defined by an interaction volume and emits either secondary electrons (SE) or backscattered electrons (BSE), which yield topographical or atomic number and phase difference information,[89] respectively. This is due to the difference in origin of these 2 types of signals: whereas the SE are emitted by the surface atoms when their electrons become excited enough to escape said surface, the BSE emerge from deeper within the interaction volume due to elastic scattering and depend on the size of the nucleus. It is apparent, then, why SEs are ideal for high-resolution surface images and BSE yield information concerning the chemical composition.[89]

Since graphene is a monolayer of carbon atoms, it is highly transparent to high energy electron beams making low energies preferable when imaging. As such, a 3.0 kV accelerating voltage was used with a SEM[90] throughout this work which enables bi/multi-layer, edge contrast and surface roughness using either the SEs from the underlying substrate (Fig. 3-2 (a)) or the graphene itself (Fig. 3-2 (b)-(c)).

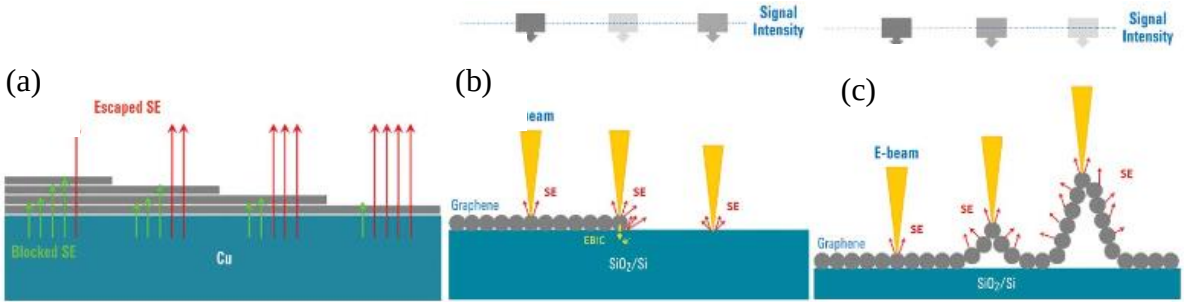

Figure 3-2 (a) Multilayer contrast shown as a function of "blocked" SEs due to multilayers. The more are blocked the fewer emerge to the detector yielding a darker contrast. (b-c) Less diffuse SEs means more of them being detected which results in a lighter contrast for the specified region. Reproduced with permission from ref. 88. Agilent Technologies, copyright 2012.

When the growths are partial, a very noticeable contrast arises between the patches of graphene and the copper substrate (Fig 3-3). Nevertheless, it is still difficult in this case to be certain that these are only partial growths as opposed to a full monolayer with bilayers forming. This is easily verified *via* Raman spectroscopy.

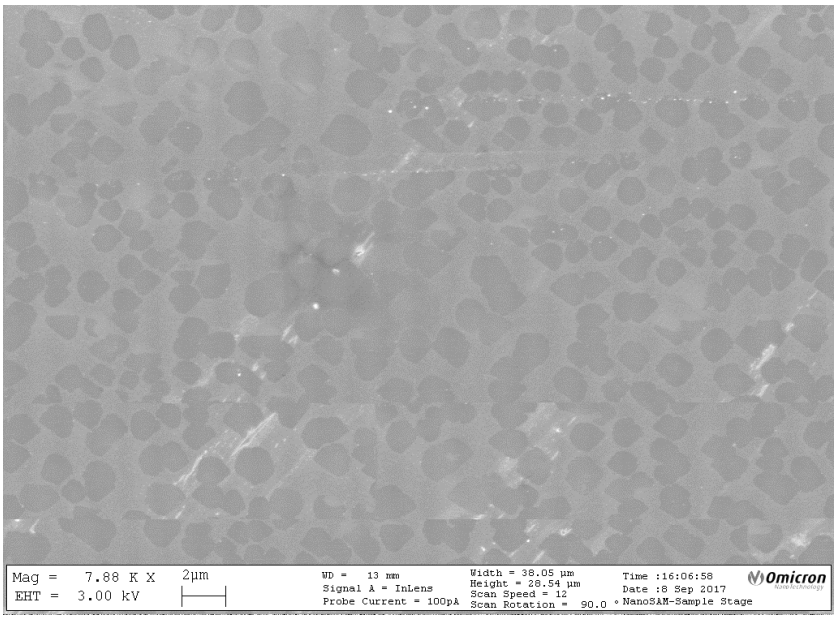

Figure 3-3 Batch 120 showing a partial growth with the graphene grains

3.3.2 **Raman Spectroscopy**

By illuminating a sample via a laser of visible light, inelastic scattering occurs that results in the emitted photons' energy to be shifted up or down. It is this energy shift that provides a

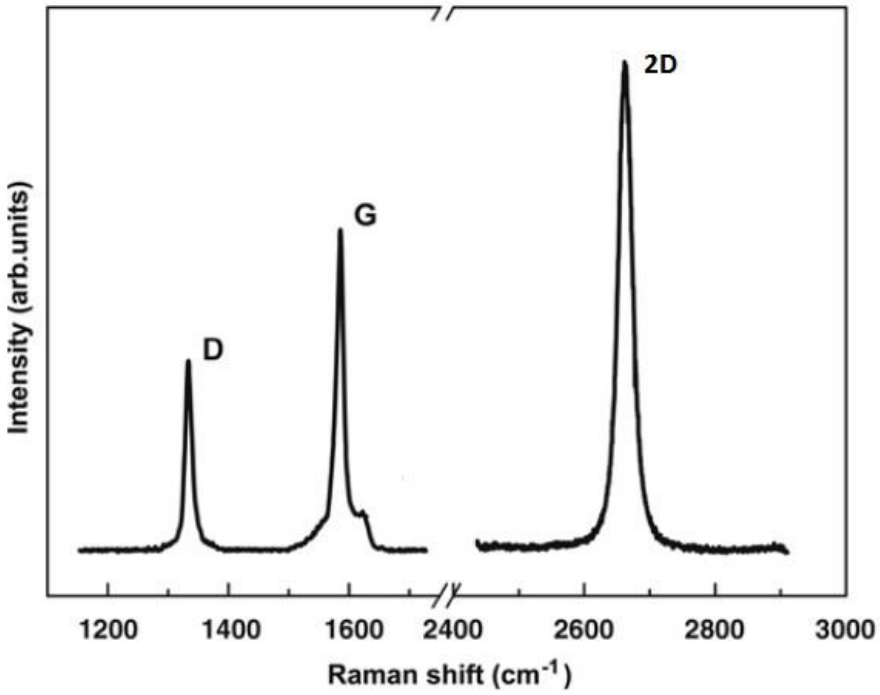

Figure 3-4 Typical Raman peak position of the D, G and 2D peaks. Reproduced with permission from ref. 92. Elsevier, copyright 2009.

structural fingerprint by measuring the vibrational modes of a molecule that makes Raman a great characterization tool. With the popularity of graphene growing upon first isolation, a quick non-destructive method was needed to assess the structure and quality. Though there are a few peaks which are unique to graphene, elucidated upon in 2006,[91] graphite had been studied via Raman spectroscopy for a long time prior to this.[92] There are 2 main peaks of interest in carbon materials: the so-called G and D peaks which lie around $1560\ cm^{-1}$ and $1360\ cm^{-1}$, respectively (Fig. 3-5). The G-band arises from the C-C bond stretching while the D arises from disorder/defects of the sp^2 hybridization (of which graphene is, ideally, wholly composed). Unique to graphene is the so-called 2D mode, which is found at around $2700\ cm^{-1}$ (Fig. 3-4). This feature is a second-order two-phonon process to be used, in conjunction with the G peak, as a quick indicator of the number of graphene layers.

Typically, a $2D/G$ ratio >1, =1 and <1, means monolayer graphene, bilayer and multilayer,

is present, respectively. However, other methods can be used to determine the number of layers including G peak position and the 2D full-width half-maximum (FWHM).[91,93] These simple ratios can be used as a quick way to determine the quality of the graphene with respect to the number of layers (with the D peak being used as an indicator of general quality *via* defects) which can then be verified by taking into account the FWHM of the 2D peak and G peak position

3.3.3 **Image Analysis**

The bulk of the information extracted from our growths was done via a SEM. While this can be done by simply counting things like nucleation densities, this can sometimes be a daunting task for growths with the number of nuclei extending to the 1000s. Therefore, for some of the image analysis – the nucleation density, the coverage percentage and the average grain size – we turn to a program called ImageJ which is a "public domain, Java-based image processing program developed at the National Institutes of Health".[94]

The first step is to analyze the grey level to differentiate the substrate from the graphene via the *Threshold* (Fig. 3-6 (a)) function which, according to the threshold we select, separates the image into black (the values of grey above the threshold selected) and white (the values of grey below the threshold selected). Next, we give greater uniformity to the image by using a function called *Noise* → *Despeckle* (Fig. 3-6 (b)) which replaces the pixels in a 3x3 matrix to the darkest of the region. Depending on the geometry and the degree of coalescence, an intermediary step may be required which uses the *Watershed* function, which was created with the express purpose of separating particles that touch with best results coming from convex geometries. Lastly, with the *Measure* function, which sums the pixels and relates them to a scale set by the user (i.e., using the scale bar at the bottom of the image), we now have the information desired: nucleation density, coverage percentage and average grain size. It does this by summing the pixels above the threshold and relating this to the total area covered by the image.

The bulk of the characterization was done with the SEM since most of the relevant information desired is obtained through analysis of partial growths - nucleation density, grain size, coverage – which is lost or rendered useless once the growth is complete, for obvious reasons. In some circumstances due to the inherent ambiguity associated with homogeneous contrasts, it is difficult to know whether the growths are full or empty (Fig. 3-5). In such situations Raman

spectroscopy was used to quickly determine whether graphene was present by looking for 2D or G peaks.

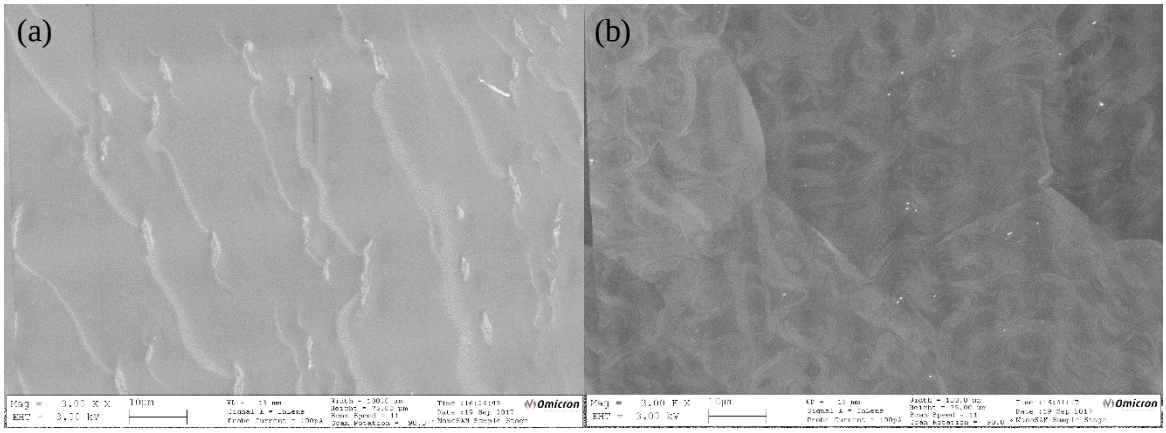

Figure 3-5 Two SEM images showing homogeneous surfaces demonstrating the utility of Raman spectroscopy. (a) Empty (bare Cu) (b) full.

This chapter showed the setup used for the graphene growths used in this thesis as well as the characterization methods – primarily the SEM with some uses of Raman spectroscopy, as needed. It cannot be overstated: while many research groups have the necessary equipment to conduct LPCVD, our particular attention to gas-phase impurities, through the use of purifiers, allows our system and measurements to remain above the "noise" threshold – a result of a poor control of said impurities.

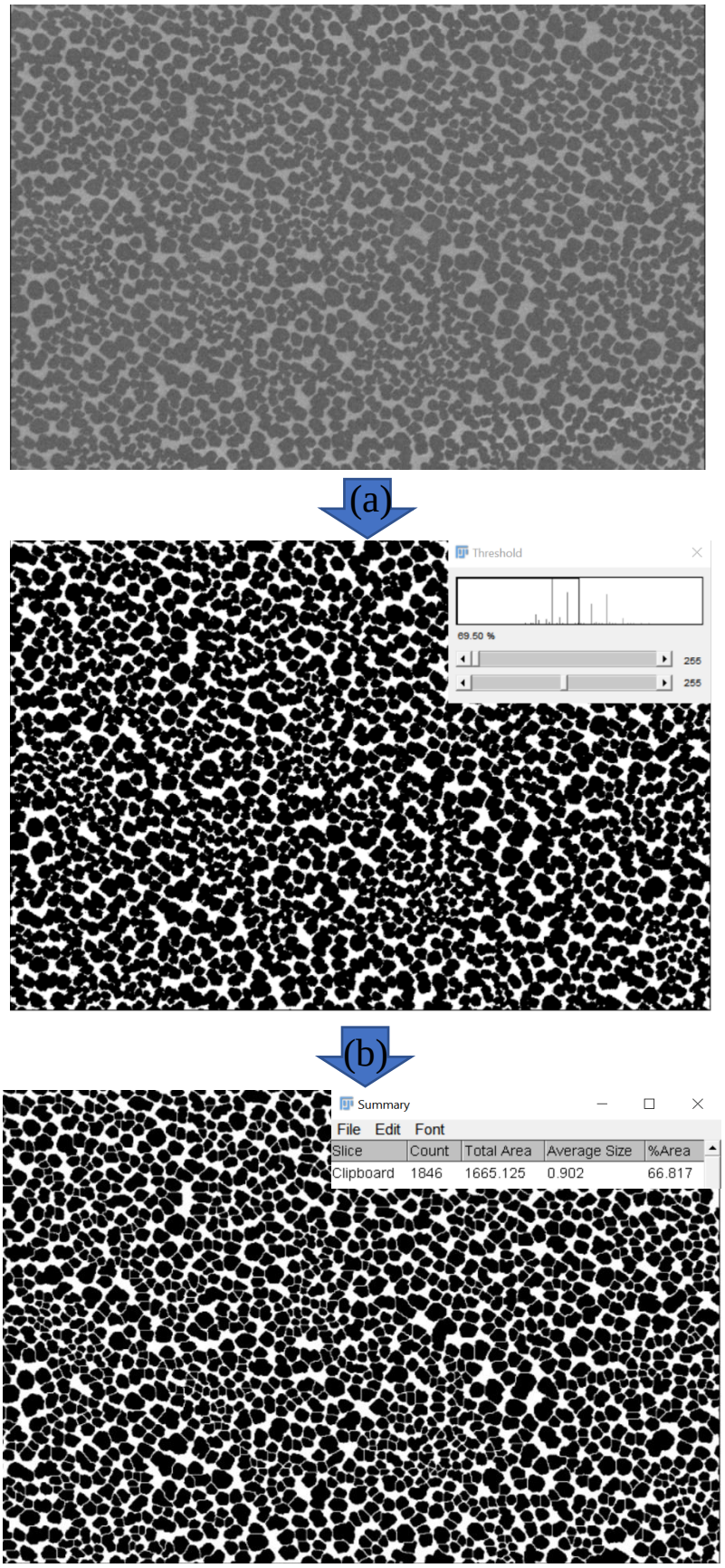

Figure 3-6 with the raw image (a) we set the ‘Threshold’ and ‘Despeckle’ and (b) add the ‘Watershed’ and ‘Summarize

CHAPTER 4 MODEL

In this chapter we formally present our model which explains the phenomena responsible for a reduction in nucleation, thus enabling large-area grains and the absence of bilayers. This model serves as the backbone of our work as most experiments were done with it in mind.

With recent investigations on bulk carbon[70] and oxygen purification,[23] we became interested in the oxygen's form (e.g., as a surface oxide and the type of oxide, as molecular oxygen which works in way in the copper, etc.) and the associated dynamics. Upon closer inspection, the phase-diagram itself suggested that a copper oxide at this temperature and pressure range ($\sim 5x10^{-5}\ Torr$) wasn't possible. This curiosity led to some back of the envelope calculations related to carbon diffusion out of copper and purification of bulk-carbon by O_2, which eventually became more pointed and ultimately led to us looking for ways to optimize and increase the "purifying power" of oxygen. The result which directed our investigations is what is presented in this section.

4.1 Copper-Carbon Phase Diagram

As has been mentioned previously, a large part of this study involves the C-Cu system not because of the actual graphene synthesis, which is surface mediated, but because of these carbonaceous inclusions as bulk impurities which we suggest play an important role in graphene growth. That is to say, and put more succinctly, while the catalytic action of methane dehydrogenation is surface mediated, the bulk still plays an important role in the early stages of growth (i.e., nucleation) due to the carbonaceous impurities, which are within the copper bulk *in spite of* its inherently low carbon solubility, and on bi/multi-layers after the initial nucleation. The former, as we will demonstrate shortly, is related to the mobility of carbon in copper where the carbonaceous inclusions work their way to the surface, in a way similar to nickel, and contribute to the nucleation by a phenomenon we name *post-nucleation*, that is, a nucleation that occurs after the surface-mediated nucleation due to methane dehydrogenation.

Taking the carbon content into account regarding nucleation is problematic for a few reasons. For one, using Alfa Aesar 99.8% copper purity only assures this purity in metal-basis and gives no insight into the kind of organic impurities, particularly carbon. Secondly, due to the long-known fact that the carbon solubility of copper is low, there has been a limited amount of work

done on the purification and characterization fronts. Therefore, we have devised a way to purify the copper substrate through a gaseous procedure *via* the introduction of molecular oxygen as a pre-treatment step to the growth (see Ch. 3) based on the copper-oxygen phase diagram.[95] An important aspect of the pre-treatment is, therefore, understanding the interaction between copper and oxygen and their relation to temperature and pressure. As can be seen from Fig. 4-1, there are two forms of copper oxide, Cu_2O (cuprous oxide) and CuO (cupric oxide). At the temperatures most graphene synthesis is done ($1000°C+$), there would not be any kind of oxide - unless very high into the APCVD regime. The first portions of the model deal with the kinetics of oxygen and carbon in copper. The second portion elaborates a way to exploit the Cu-O phase diagram for a better purification process.

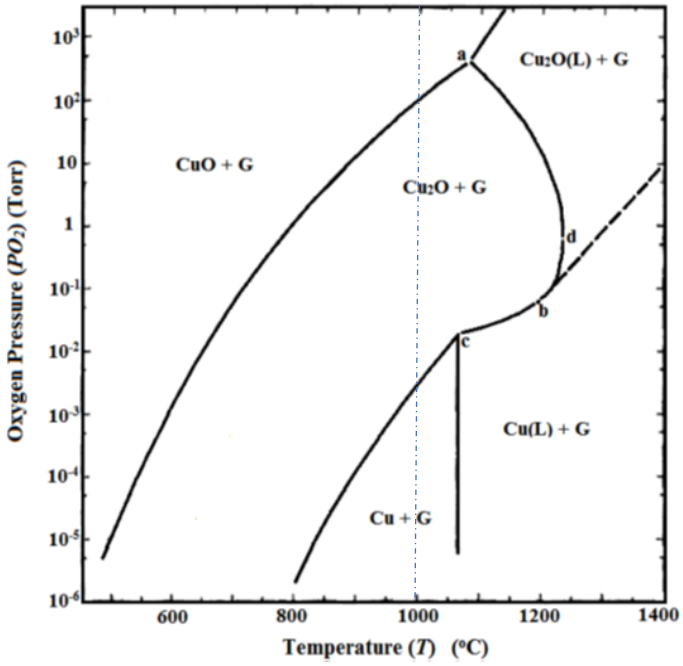

Figure 4-1 Copper-oxygen phase diagram where "L" and "G" standard for "Liquid" and "Gaseous", respectively. Reproduced with permission from ref. 93. Elsevier, copyright 1974.

In much the same way that our research group's past work dealt with threshold levels of gas impurities and their unexpected impact, this work elaborates on the impact of something thought to have played no role in nucleation previously. In fact, the idea that the solubility of carbon in copper is too low to be meaningful probably heavily contributed to it being an overlooked element.

We first set the stage: recent work has suggested that the carbon content in copper lies between 0.5 – 240 ppm. A typical nucleation density for a standard growth is $\sim 10^6$ nuclei$/cm^2$, which has been reduced to less than 1 nuclei$/cm^2$ using an oxygen pre-treatment at $P_{O_2} = 1x10^{-5}\ Torr$ for 60 minutes to yield graphene grains of size $1\ cm^2$. Additionally, the surface carbon concentration must reach $5x10^{13}\ atoms/cm^2$ before saturation and nucleation occurs. Using this experimentally determined carbon content of 0.5 – 240 ppm, back-of-the-envelope calculations show between 11 and $0.025\ \mu m$ of copper would need to be evaporated – which would take between 220 min and 30 s – for enough carbon to segregate at the surface for nucleation to occur given the carbon concentration mentioned. The length of time required already suggests that something towards the higher end is more plausible.

Next, we consider methods to diminish the nucleation by a factor of 10^6, which requires a reduction in carbon concentration (c_c) within the copper of $\frac{C_C}{C_{0C}} < 1x10^{-3}$, where c_{0c} is the initial carbon concentration. We begin by considering the system as a 1D problem and solve the diffusion equation with the copper foil of thickness L of carbon concentration C_{0C} and wish to solve for the amount of time necessary to obtain the desired purification. Using the appropriate boundary conditions, a time of 3.6 seconds is necessary to reduce the carbon concentration by $1x10^{-3}$. Next, we calculate the rate of initial carbon consumption per unit area. For the above stated reasons, we assume a carbon concentration of 240 ppm and a homogeneous mid-foil $\left(\frac{L}{2}\right)$ rate of consumption, i.e., equal throughout. The probability of having an oxygen atom collide with a surface carbon is calculated to be $4.18x10^{11}/cm^2$. Compared to the variation of carbon diffusion from the bulk to the surface of $\frac{dn_C}{dt} = 6.5x10^{12}/cm^2$, the estimate demonstrates that there aren't enough direct collisions with the surface carbon to remove the bulk carbon (in the ideal approximation that the reaction rate is unitary). This result suggests that the purification of the copper foil is collision-rate limited and that the time of purification must be superior this lower bound. Given this regime, we start by assuming that the distribution of carbon in copper c_C is uniform within the copper foil (such that $C_C(x,t) = C_C(t)$) so that the number of carbon atoms removed will be proportional to the impingement rate Z_{O_2}, by the probability of hitting a carbon atom, and modulated by the reaction coefficient $f = 0.01$. The time to attain the desired bulk and surface purification is of 12.8 min, which is shorter than the experimentally observed time of 60 min. Given this value, it is possible

to suggest that the carbon content is greater, however, we here suggest that the carbon content is not in atomic form but, rather, in a graphitic form which will limit the reaction between oxygen and these graphitic inclusions. Next, we attempt to demonstrate a way of ridding ourselves of these carbonaceous clusters. We begin by noting that a cupric oxide, Cu_2O, is formed at $700°C$ which does not happen at $1000°C$. Given this oxide, the oxygen concentration at the surface will be $[O] = 0.33$ which will diffuse with coefficient $D_0(700°C) = 5x10^{-10}\ m^2/s$. Given a copper concentration of $C_{Cu} = 8x10^{22}\ Cu/cm^3$, an oxygen concentration of $2.64x10^{22}\ O_2/cm^3$ is found. On the other hand, at $1000°C$ with no oxide present, a diffusion coefficient of $D_0(1000°C) = 3x10^{-9}\ m^2/s$ with an oxygen concentration of $[O] = 8x10^{10}\ /cm^3$. Noting the general relationship $\frac{dC_0}{dt} \propto C_{0O} \cdot D$, despite losing an order of magnitude in flux due to the decrease in D, this is more than compensated by the 11-fold gain due to the oxide present.

The argument is subtle and can be easily missed. Firstly, lower bounds, either for diffusion of carbon throughout the copper sample or a time-frame for the oxygen to help in the purification process. In fact, these are so underestimated in comparison to what is seen that it leads us to our conclusion and model: the carbon within the copper bulk is not in atomic form but, rather, in sequestered groupings of carbon which is more stable, and therefore takes longer to react with the oxygen and out-diffuse from the bulk. To optimize the purification, we show that a process involving a temperature at which Cu_2O is formed greatly helps, something that is demonstrated in the results section next.

The above-detailed model and its graphical representation (Fig. 4-2) offer important and unique insight into graphene nucleation and growth that have not yet been clued into by the scientific community. That there are graphitic bulk-bound carbonaceous impurities present and that its role in nucleation has been ignored or underestimated was done to the detriment of the progress in graphene synthesis. With our purification procedure these are able to be eliminated and nucleation can be represented much more faithfully solely in relation to the methane flux.

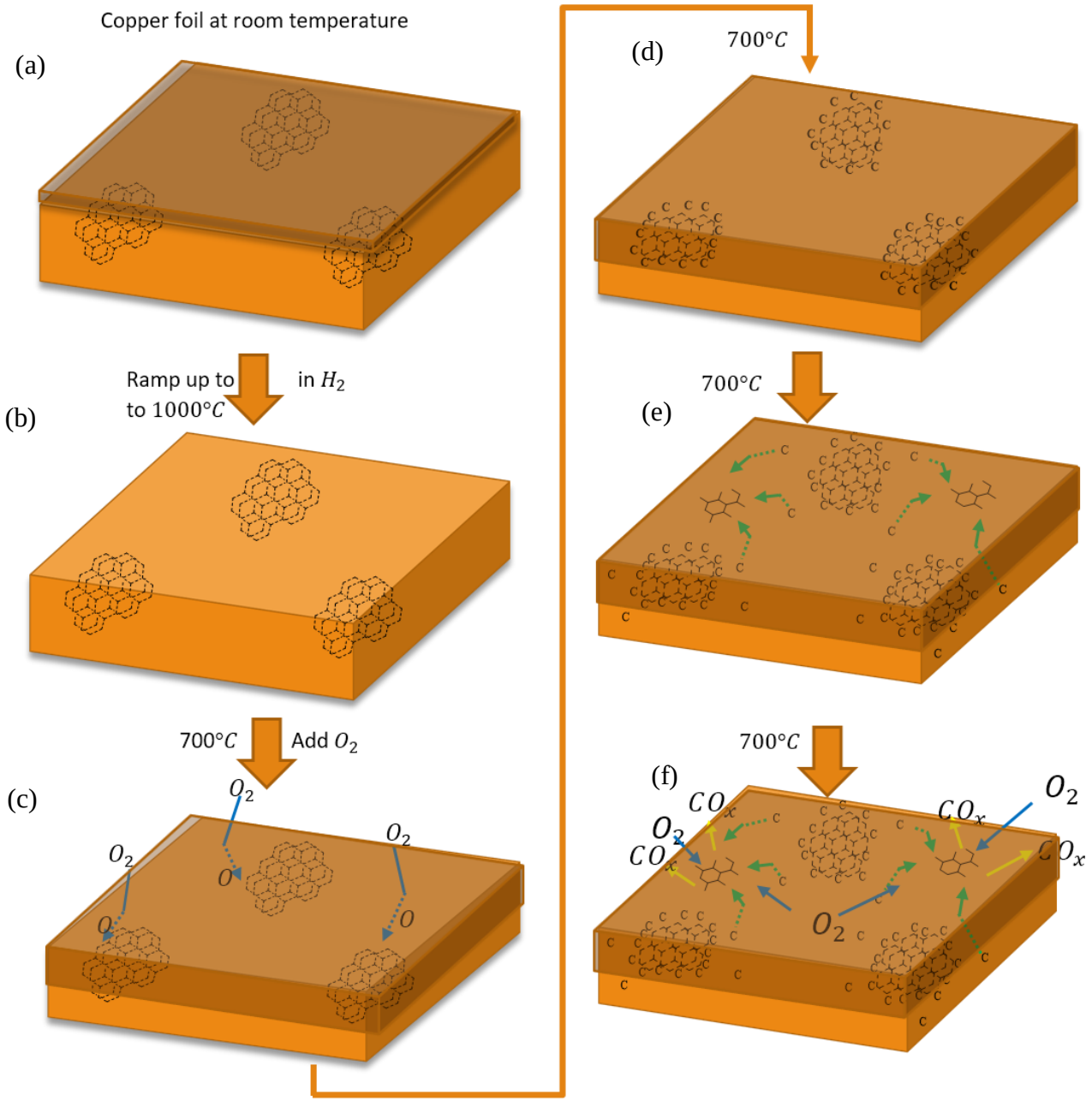

Figure 4-2 Graphical representation of the model for copper pre-treatment. Darker orange represents copper oxide. a) Copper foil at room temperature after cleaning pre-treatment will still have a very thin oxide layer which is b) removed during the ramp up to 1000°C in a hydrogen environment. c) Once desired temperature is achieved, the temperature is set to 700°C, H_2 is removed and O_2 is introduced which diffuses into the copper bulk and reacts with these carbonaceous inclusions which d) are slowly etched from the perimeter into an atomic carbon cloud surrounding these inclusions. e) The atomic carbon will diffuse to the surface from where it f) reacts with the oxygen and leaves as CO_x.

CHAPTER 5 RESULTS

In this chapter we present the relevant results pertaining to this document. The bulk of the data is qualitative in nature so that much of the time spent analyzing the images has more to do with following the line of thought within the respective series and relating the changes to a causal explanation of which the model we've presented is the proposed candidate.

Showed below is Table 5-1 which summarizes the results of this thesis regrouped by "series", that is to say, a series or number of graphene growths which explore an idea within said series but are not interrelated to one another, though may, in some circumstances, help lend credence and support. The results are summarized in sequential order from left to right, i.e., the "anneal" before the "growth" which then yield "results" upon characterization and analysis. The "anneal" portion first presents the gas order sequentially from left to right followed by the time "t" of anneal in the same order so that "$O_2/H_2/O_2$" "30/30/0" signifies an anneal in O_2 for 30 minutes followed by an anneal in H_2 for 30 minutes finishing with an anneal in O_2 for 0 minutes at the temperature T (of which all the growths are done at the same temperature as the annealing temperatures). Next, the growth section has the methane pressure in "Torr" followed by the dose, from which the time can be deduced since the dose is simply a multiplication of the methane pressure by the time. Lastly, the results section presents the density of nucleation followed by the average area of graphene grains obtained, ending with the percentage of the surface area that is covered by graphene.

Table 5-1 Table summarizing the graphene growths of this thesis grouped by series numbers The "gas order", "time" and "temperature" are all specific to the annealing conditions with the P_{CH_4} and CH_4 dose to the growth phase. All growths are carried out at $1000°C$.

		Anneal			Growth		Results		
Series	Sample #	Gas Order	t (min)	T ($°C$)	P_{CH_4} (Torr)	CH_4 Dose	Density (μm^2)	Avg. Size (μm^2)	Coverage (%)
1	B138	$O_2/H_2/O_2$	30/30/0	1000	$3.5x10^{-3}$	0.05	0.59	1.1	65
	B139	$O_2/H_2/O_2$	30/30/1	1000	$3.5x10^{-3}$	0.05	0.028	11.76	33
2	B120	$H_2/O_2/H_2$	30/20/5	1000	$3.5x10^{-3}$	0.18	0.21	2.1	46
	B121	$H_2/O_2/H_2$	30/10/5	700	$3.5x10^{-3}$	0.28	0.08	55.8	39
	B123	$H_2/O_2/H_2$	30/20/5	700	$3.5x10^{-3}$	0.28	0.0045	85.2	39
	B124	$H_2/O_2/H_2$	30/40/5	700	$3.5x10^{-3}$	0.28	0	0	0
3	B119	O_2/H_2	25/5	1000	$3.5x10^{-1}$	0.21	$1.4x10^{-1}$	860	28

5.1 Series 1 – Surface Bound Carbon (B138 & B139)

The first series of experiments was done within the context of disentangling and demonstrating certain aspects of the model, mainly, the impact of the carbonaceous inclusions on nucleation once surface-bound. This study is composed of 2 growths with only one growth parameter differentiating them: an additional minute of oxygen at the end of the annealing to fully remove the surface-bound carbon originating from the bulk.

We first begin with a summary of the results for Series 1 followed by the growth parameters from ramp up to the synthesis of the graphene. It is worth clarifying that the "anneal" step consists of 2 gas sequences. First an oxygen phase for 30 minutes followed by another 30 minutes of hydrogen while the "growth" phase has both process gases flowing simultaneously.

Table 5-2 Summary of the growth characteristics for Series 1. Highlighted in red is the impact of an additional minute of oxygen at the end of the annealing sequence on nucleation density, average size and coverage percentage, compared to no additional annealing step. Both growths were done at $1000°C$

Sample #	t^{O_2} (min)	Density (μm^{-2})	Avg. Size (μm^2)	Coverage (%)
B138	0	0.59	1.1	65.11
B139	1	0.028	11.76	33

Table 5-4 Growth parameters for Series 1 highlighted in white is constant for both growths while the step highlighted in red is unique to (b), the red-bordered growth in Fig. 5-1.

	Ramp up		
1 hour	H_2	$5x10^{-2}\ Torr$	To $1000°C$
	Anneal		
30 min	O_2	$5x10^{-5}\ Torr$	$1000°C$
30 min	H_2	$5x10^{-2}\ Torr$	
1 min	O_2	$5x10^{-5}\ Torr$	
	Growth		
	H_2	$5x10^{-2}\ Torr$	
10 sec	CH_4	$3.5x10^{-3}\ Torr$	$1000°C$
	Dose = 0.05 Torr		

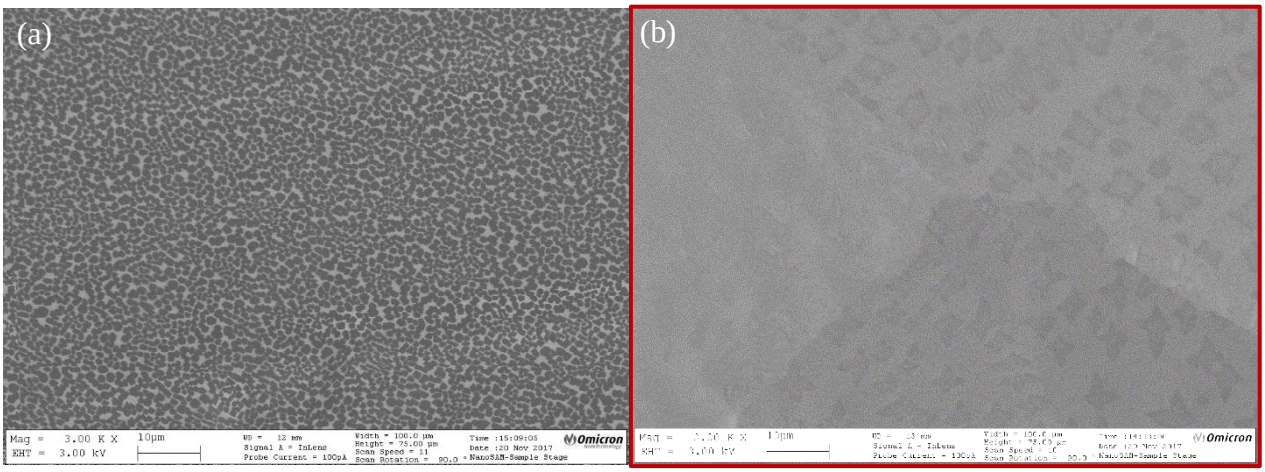

Figure 5-1 Series 1 growths showing the control growth (a) and the impact of (b) an additional 1 min O_2 gas step at the end of the annealing sequence.

As can be readily seen in Table 5-3 and Fig 5-1, by ridding the surface of bulk out-diffused carbon a decrease in graphene nucleation density from 0.59 to 0.028 μm^{-2} results in a 10-fold increase in the average graphene grain size from 1.1 to 11.76 μm^2. This results in a 2-fold decrease in graphene coverage from 65% to 33%.

5.2 Series 2 - Cu_2O Formation and Purification

The following three growths aim to study the role of the cupric oxide formation (Cu_2O) on graphene nucleation. To encourage this formation, an oxidation process was done at $700°C$ with its duration doubled for each growth starting from 10 minutes (i.e., 10, 20 and 40 minutes).

The first of these growths serves to establish a baseline by which the following 3 growths can be compared against. Therefore, all the growth parameters are identical save for the annealing which does go down to $700°C$ but still has an oxygen annealing phase at $1000°C$. In this way, we hope to be able to highlight the direct impact of annealing at $700°C$ *vs.* $1000°C$ in addition to investigating the impact of the anneal at $700°C$ as a function of time. It is worth noting that the oxygen pressure was maintained during the ~13 min ramp up from $700°C$ to $1000°C$ to avoid a reduction of the oxide itself until desired.

Table 5-3 Summary of the growth characteristics (density, average island size and coverage percentage) for series 2

Sample #	t^{O_2} (min)	Temp. ($°C$)	Density (μm^{-2})	Avg. Size (μm^2)	Coverage (%)
B120	20	1000	0.21	2.1	46
B121	10	700	0.08	55.8	39
B123	20	700	0.0045	85.2	39
B124	40	700	0	0	0

Table 5-4 Growth parameters for series 2. Ramp up, ending of annealing phase and growth parameters are universal for all growths while the colors pertain solely to the similarly colored growths in Fig 5.2

	Ramp up		
1 hour	H_2	$5x10^{-2}\ Torr$	To $1000°C$
	Anneal		
20 min	O_2	$5x10^{-5}\ Torr$	$1000°C$
10 min + ramp up to $1000°C$	O_2	$5x10^{-5}\ Torr$	$700°C$
20 min + ramp up to $1000°C$	O_2	$5x10^{-5}\ Torr$	$700°C$
40 min + ramp up to $1000°C$	O_2	$5x10^{-5}\ Torr$	$700°C$
5 min	H_2	$5x10^{-1}\ Torr$	$1000°C$
	Growth		
	H_2	$5x10^{-2}\ Torr$	
90 sec	CH_4	$3.5x10^{-3}\ Torr$	$1000°C$
	Dose = 0.28 Torr		

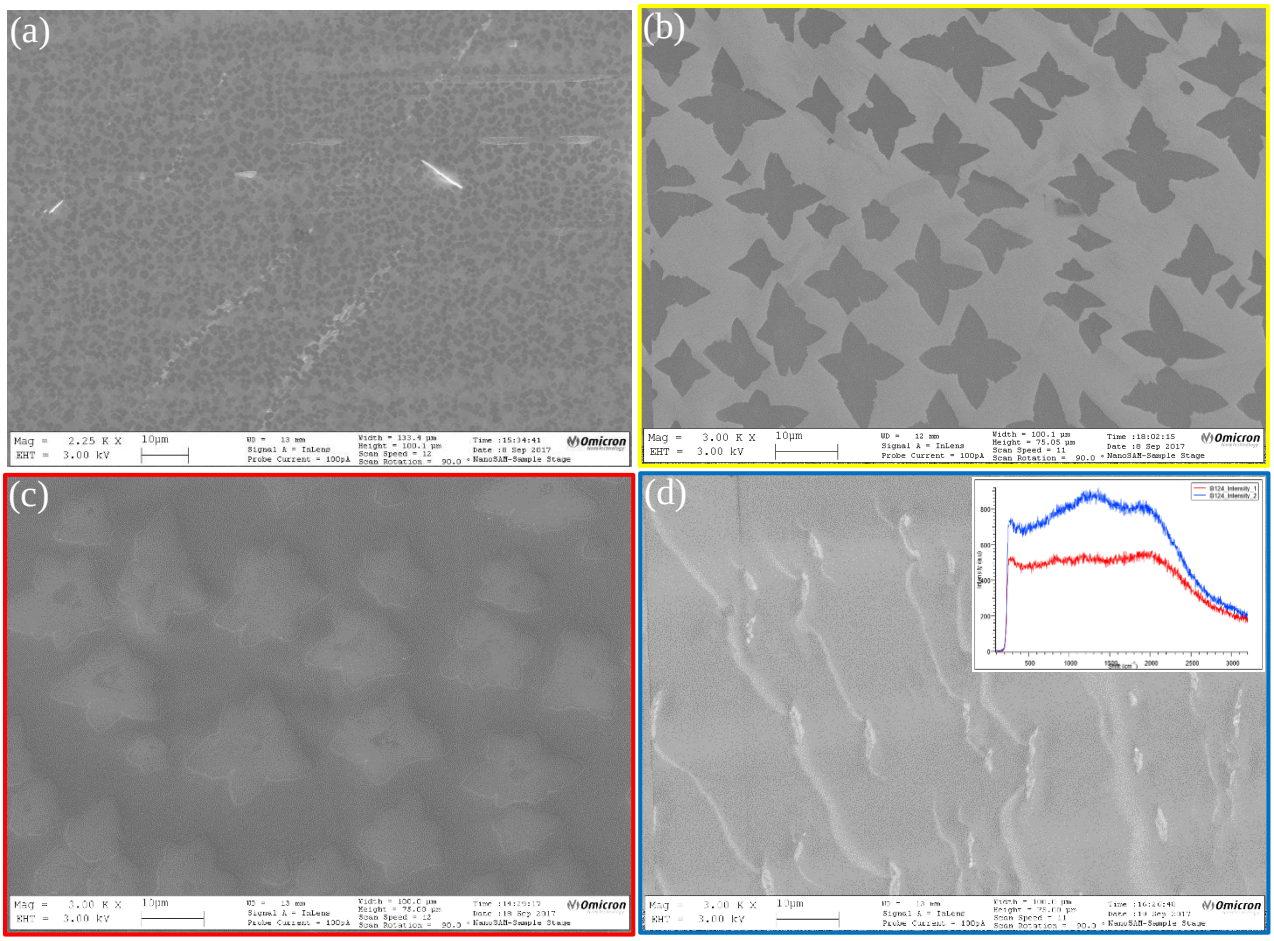

Figure 5-2 Series 2 growths showing the difference in graphene nucleation of (a) B120 (b) B121 (c) B122 and (d) B123. Annealing times of (b) 10 minute (c) 20 minute and (d) 40 min at $700°C$. Inset of (d) shows a wavenumber vs intensity Raman spectrum taken at two different locations.

A decline in nucleation density due to the increased annealing time at $700°C$ can be readily seen by comparing B121 with a 10 minute O_2 anneal and B123 with a 20 min anneal, from 0.08 to 0.0045 μm^{-2}, until complete quenching is achieved at 40 minutes seen in B124 (Fig. 5-2 (b)-(d) and Table 5-3), corroborated with 2 Raman spectra at different locations with a clear lack of graphene signature (inset Fig 5-2 (d)). This reduced nucleation allows for larger graphene grains to occur, from 55.8 to 85.2 μm^2, with an identical coverage of 39% until full quenching, which brings the coverage to 0. Additionally, a comparison between B120 and B123 (Fig 5-2 (a) and (c)) shows a dramatic reduction in density, from 0.21 to 0.0045 μm^{-2}, and increase in average graphene grain size from 2.1 to 85.2 μm^2. These two growths are compared as they both underwent the same annealing time at the same oxygen pressure but at different temperatures ($1000°C$ and $700°C$) to

give a sense of difference in carbonaceous removal ability at the respective temperatures, or more directly, at a temperature range (given our oxygen partial pressure) where an oxide is formed.

5.3 **Large-Grain**

Lastly, we present here preliminary, but promising, results regarding large-grain growth of graphene.

Table 5-5 Growth parameters for the large grain growth B119. Argon diluted with 10 ppm oxygen is added during growth phase.

		Ramp up	
1 hour	H_2	$5x10^{-2}\ Torr$	To $1000°C$
		Anneal	
25 min	O_2	$5x10^{-5}\ Torr$	$1000°C$
5 min	H_2	$5x10^{-1}\ Torr$	$1000°C$
		Growth	
	H_2	$5x10^{-2}\ Torr$	
90 sec	CH_4	$3.5x10^{-4}\ Torr$	$1000°C$
	Ar_{10ppm}	$1x10^{-1}\ Torr$	
		Dose = 0.21 Torr	

Of note, the argon added during the growth is a mixture of 10 ppm oxygen (plus ~1ppm inherent to UHP Argon oxygen impurities) in argon so that

$$P_{Ar(11ppm)} = 1x10^{-1}\ Torr$$

yields an oxygen partial pressure of

$$P_{O_2} = 1.1x10^{-6}\ Torr$$

which puts us in the approximate ball-park of standard (i.e., without additional purifiers) LPCVD grown graphene using standard UHP CH_4 (5ppm O_2 impurity) and H_2 (1ppm O_2 impurity): $P_{O_2} = 5x10^{-2}\ Torr \cdot 6ppm = 3x10^{-6}\ Torr$. This back of the envelope calculation is at the heart of Choubak's studies[83,84] which shows the benefit of purifying the UHP gases as described at the end of Chapter 2.

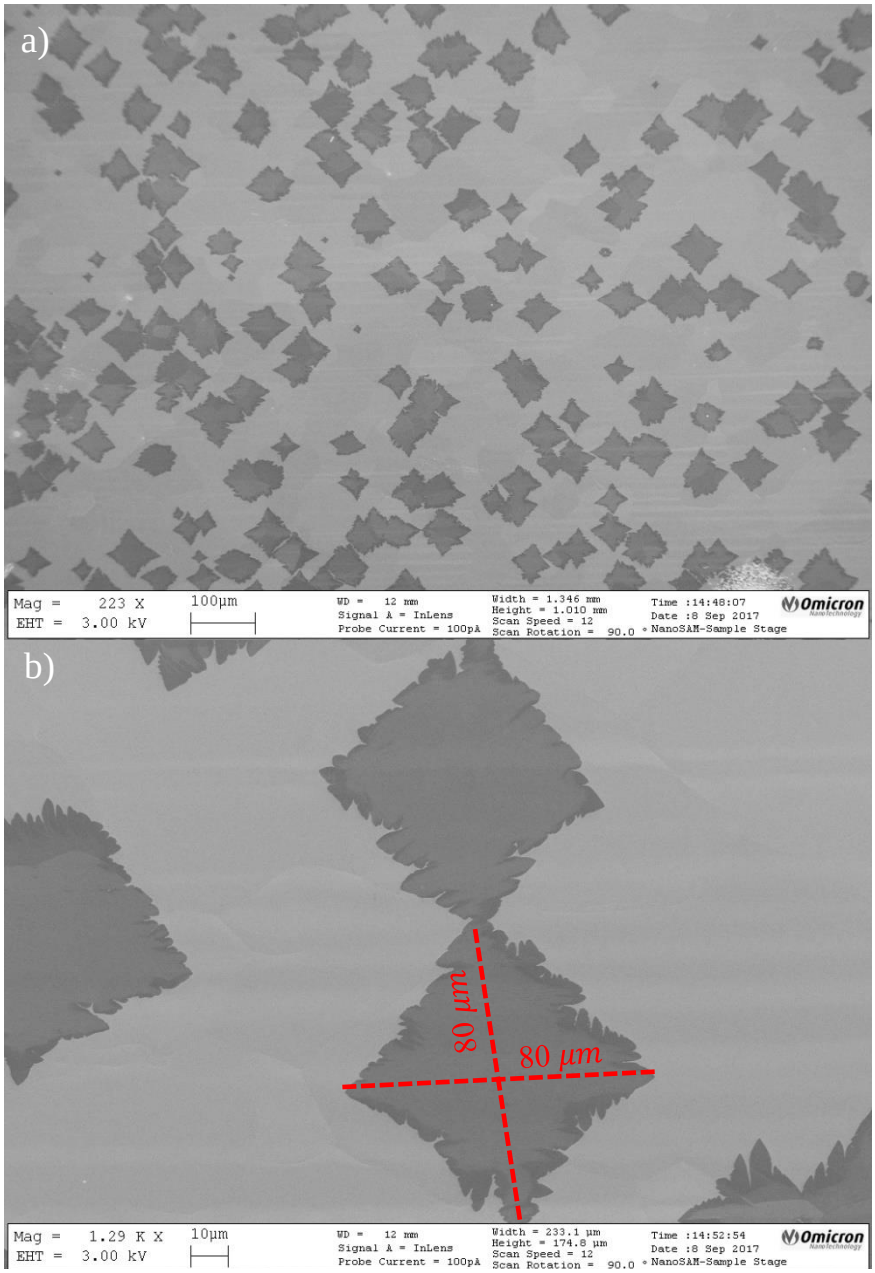

Figure 5-3 SEM micrograph of B119, the large area graphene growth. (a) A low coverage (due to low nucleation density) enables large area grains up to (b) 80x80 μm.

Table 5-6 Growth characteristics for large-area graphene growth B119.

Sample #	t^{O_2} (min)	Density (μm^{-2})	Avg. Size (μm^2)	Coverage (%)
B119	25	$1.4x10^{-4}$	860	28

The 10 ppm oxygen diluted in argon yielded the largest graphene grains obtained to date within our research group with an average grain size of 860 μm^2 which had ample room to grow, evidenced by the 28% coverage, due to the extremely low nucleation density of $1.4x10^{-4}$ μm^{-2} (Fig. 5-3 and Table 5-6).

5.4 **Post-nucleation**

Mentioned very briefly in Chapter 4, there seems to be very little information or research related to what we refer to here as "post-nucleation", that is, the nucleations which happen after the first nuclei form. In this sense, these "generations" of nucleation can be viewed as a sort of "strata" in an archeological sense, that could conceivably "date" groups of nucleations according to their size (Fig. 5-4). We attempt to establish a connection between the size of nucleation groups, or generations, and time, such that nuclei from generation "G_1" would have begun at a time "t_1", and so on. This is information that is accessible in our case because of the carbon gettering procedure *via* oxygen pre-treatments which makes it such that all nucleations are directly linked to the methane flux which eliminates nucleations due to out-diffusing bulk-carbon which would act as a sort of noise by muddying the waters. It's worth noting that the above statements simplify

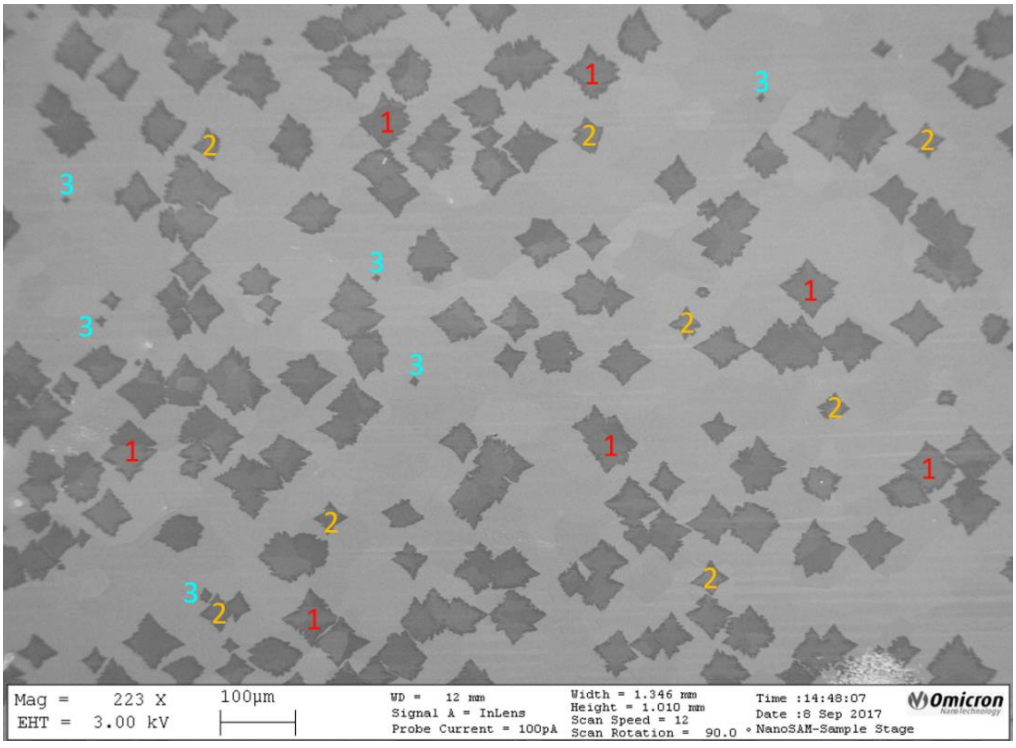

Figure 5-4 B119 showing three different graphene nucleation generations with 1 having nucleated first and 3 having nucleated last.

nucleation and growth in a way that probably doesn't do it justice, though perhaps some insights can still be obtained from this oversimplification. A full and proper analysis of this kind would also take into consideration, amongst other things, distance to nearest-neighbor, since these grains compete against one another for the carbon adatoms as a fuel for lateral growth. The lower left area has two clear 1st generation islands next to one another with 3rd generation islands growing both next to 2nd generation islands (bottom left) and in a vast area far from any grains (top right). With the help of this simplistic analysis some of the concerns may be assuaged and could lead to some meaningful results: once the carbonaceous impurities from the bulk have been removed, a much clearer picture of nucleation emerges as these nucleations are mostly dictated by the carbon precursor and not out-diffusion of said impurities, which also aides the capability of obtaining larger grains (something that will be elaborated upon further). A similar level of analysis regarding nucleation generations can equally be extended to the other growths in the results section, typically yielding 1-3 generations (though this is more of an eye test than an exact science).

5.5 **Bi-/Multi-layers**

Lastly, we present results concerning bi- and multi- layers that have historically been present but no longer appear in this work. More specifically, we refer to the previous PhD students' work, Saman Choubak, with whom the graphene work was started within this research group and use some growths from her thesis as a comparison. In this sense, this portion of the results section are negative results that emerged from careful study of the SEM images noting something rather peculiar – a lack of bi- and multi- layers. Fig. 5-5 presents the images from Saman's thesis[96] with the growth parameters presented in Table 5-7. It is impossible, within this work, to find a growth using the exact same parameters that were used. To this extent, it is difficult to know what is the most salient feature when trying to meaningfully compare previous' work with this one – should one be looking at the total time of growth, should we absolutely compare full-growths with full-growths or is it possible to compare them to partial growths? Certainly, if one feels comfortable comparing partial growths with the completed ones presented in Saman's work then one can simply browse through the multiple partial growths presented in this result section. However, for the sake

of being as close as possible we present this completed growth below with no evidence of bi- or multi-layers - one amongst many.

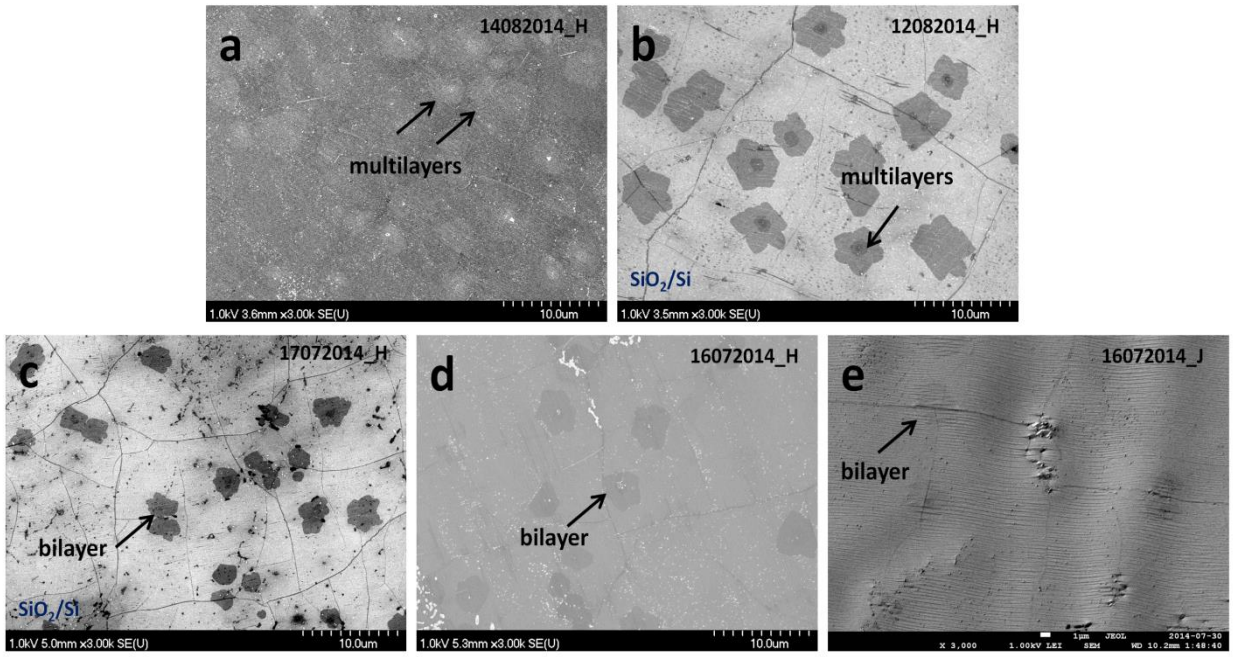

Figure 5-5 Various SEM micrographs of graphene on Cu (a, d, e) and on SiO_2 (b, c) from Saman Choubak's[94] showing presence of bi and multilayers under a completed monolayer of graphene.

Table 5-7 Growth parameters of the growths used in Saman Choubak's thesis showing a much longer growth time used resulting in a much higher methane dose.[94]

	Ramp up		
1 hour	H_2	$5x10^{-2}\ Torr$	To $1000°C$
	Anneal		
30 min	H_2	$5x10^{-2}\ Torr$	$1000°C$
	Growth		
	H_2	$5x10^{-2}\ Torr$	
30 min	CH_4	$2x10^{-1}\ Torr$	$1000°C$
	Dose = 810 Torr		

Table 5-8 Growth parameters for growth B118 which serves as a point of comparison to Choubak's growths.

		Ramp up	
1 hour	H_2	$5x10^{-2}\ Torr$	$1000°C$
		Anneal	
25 min	O_2	$5x10^{-5}\ Torr$	$1000°C$
5 min	H_2	$5x10^{-1}\ Torr$	
		Growth	
	H_2	$5x10^{-2}\ Torr$	
30 min	CH_4	$3.5x10^{-4}\ Torr$	$1000°C$
	Ar_{10ppm}	$1x10^{-1}\ Torr$	
		Dose = 0.63 Torr	

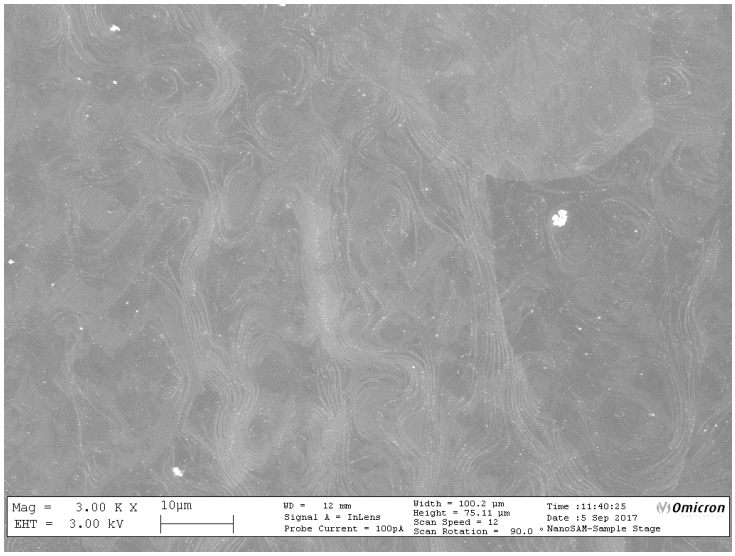

Figure 5-6 SEM micrograph of B118. A completed full layer of graphene is used as a point of comparison to Choubak's work displaying no bi/multi-layers under a completed graphene monolayer.

Next, we present the associated Raman of three different locations (Fig. 5-7). It's important to note that these spectra were obtained on copper directly, that is, the graphene was not transferred to SiO_2. Looking at the spectra we first notice the I_{2D}/I_G ratio as being less than 1 which would seem to suggest multilayer graphene (bilayer most likely). However, the position of the G band between 1588 and 1591 cm^{-1} in addition to the FWHM of the 2D band being far from what would be expected for bilayer graphene (~50) suggests that this is monolayer.[73,75]

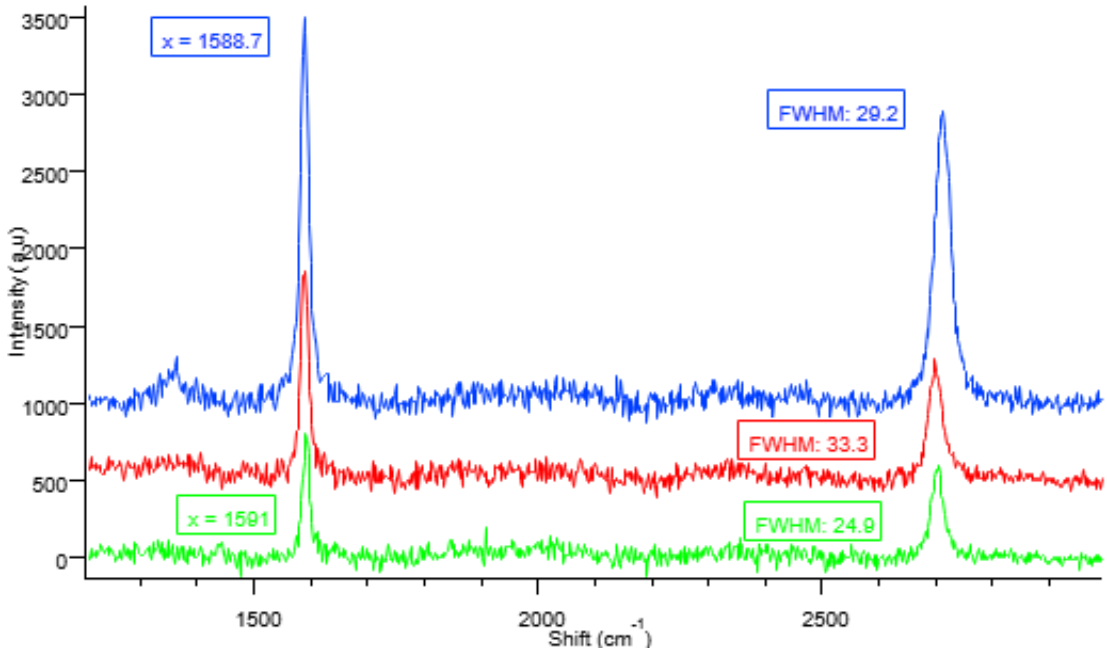

Figure 5-7 Raman spectra of B118 taken from 3 different locations of graphene on copper showing no sign of bi/multilayers from the location of the G peak and FWHM of the 2D.

CHAPTER 6 DISCUSSION

The purpose of this work was not to definitively demonstrate phenomena but, rather, to point to or elucidate an aspect of growth which has been largely ignored, that is, the impact of carbonaceous impurities found within the copper substrate which was thought to be too low to matter. To this extent, the results are poignant but preliminary – they clearly demonstrate that there are phenomena related to the bulk as opposed to surface-bound impurities, as demonstrated by the nucleation experiments. By exploiting the Cu-O phase diagram a "deeper" level of carbonaceous impurity reduction can take place with a clear impact on nucleation which also has important consequences on the formation of bi- and multi- layer graphene. In Chapter 5, interesting results are highlighted pertaining to peripheral impacts that oxygen can have, such as recrystallization of the copper surface, post-nucleation, reduced-oxide-created indentations, etc. which sets the groundwork for interpretations and understanding of the phenomena observed.

6.1 Nucleation

The first set of experiments are meant to determine the impact of surface-bound carbon on nucleation due to out-diffused bulk carbonaceous impurities. In the first growth of this study, a growth is carried out after having annealed in O_2 for 30 minutes followed by an anneal in H_2 for 30 min. It is important to note that hydrogen is a non-reducing agent on Cu surfaces during the

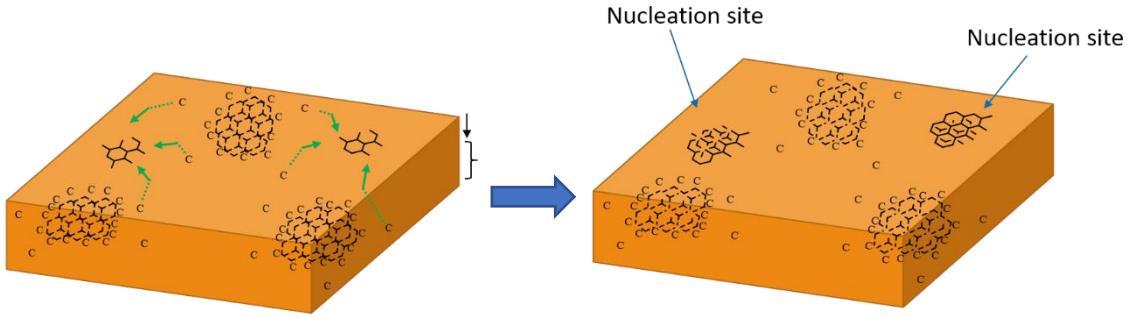

Figure 6-1 Model showing the impact of bulk carbonaceous impurities on graphene nucleation. Left graphic shows carbonaceous impurities working their way to the surface through diffusion which then aide in nucleation of graphene.

anneal phase[21] so that whatever carbon is segregated to the surface over the 30 min time-span remains and can eventually play a role in nucleation during the growth phase (Fig. 6-1). This becomes more obvious when we couple this growth with the next one in which a minute of O_2 is added (with otherwise identical parameters) at the end to remove this surface-bound carbon (Fig.

6-2) which has a significant impact on the nucleation which reduces it by a factor of 20 (Table 5-3).

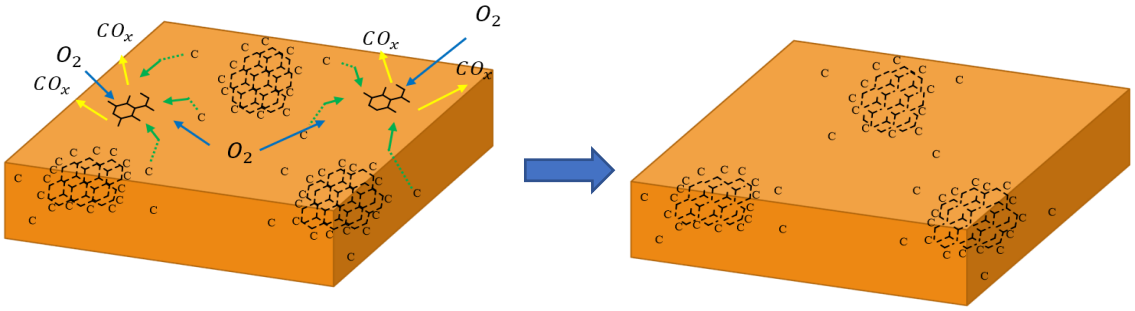

Figure 6-2 Proposed model for the impact of oxygen on the carbonaceous impurities. Left graphic shows oxygen as carbon-scavenger of surface-bound carbon. The result (right graphic) is a cleaner surface with some carbonaceous inclusions still present (depending on oxygen anneal time) though in a more broken up form than previously due to oxygen.

There is still much research that can be done related to these preliminary results. More results would be necessary to determine, for example, the time required to burn surface-bound carbon, though it's safe to say that this should happen on the timescale of seconds once in contact with the oxygen given the temperature at which graphene growth typically occurs. Moreover - and this will be an idea that will be expanded upon later – the amount of time necessary to reduce whatever oxide is present is something of an unknown with a reduction dose as a product of time and H_2 pressure is something that could be obtained. In our case, it is difficult to know how much of an oxide is present at the beginning of the growth phase being that one must be formed due to oxygen being the last step of the anneal phase and, more importantly, how much of an impact this oxide could have on nucleation.

6.2 **Oxide Formation**

The second series of experiments was meant to elucidate the impact of oxide formation on nucleation. This was done by lowering the temperature at which the O_2 anneal phase happens to $700°C$, while maintaining the oxygen partial pressure at which a cupric oxide (Cu_2O) would form (Fig. 6-3). The first growth, B120, serves as a baseline with which the following three growths −B121, B123, B124 − are to be compared with the annealing times doubled over the three growths from 10 to 40 minutes (Fig. 5-2 and Table 5-4).

To ensure that these growths proceeded unhindered, a small H_2 reduction step was done to remove the oxide present and to give time for the copper surface to re-planarize (something that will be elaborated upon later). Immediately evident, not only does the nucleation density decrease between the 10 and 20 min growths, but after 40 min of O_2 anneal the nucleation is completely quenched (Fig. 5-2). This would suggest that the nucleation density is greater when the last step of the anneal is a non-carbon-reducing one (H_2), which provides time for the carbonaceous inclusions to migrate to the surface and serve as nucleation sites (in all cases but the one where nucleation is fully quenched assuming a 100% efficiency in ridding the carbonaceous impurities). These results could lend themselves to saying that the carbonaceous inclusions have been reduced within the bulk to a sufficient degree that the surface carbon cannot attain a critical cluster size necessary to nucleate (given the CH_4 partial pressure), and, moreover, that nucleation possibly ***requires*** carbon from the bulk to provide some carbon atoms necessary for nucleation to occur. The line of reasoning proceeds as such: given a 40 min oxygen anneal phase and no nucleation given the same conditions ($5x10^{-2}$ Torr hydrogen and $2x10^{-3}$ Torr methane), what would happen to graphene nucleation given a longer growth time? If nucleation would eventually proceed, would it be due to the combined impact of evaporated copper and carbon diffusion enhancing surface segregation or would it be due to a long enough time given a statistically small likelihood of having the necessary carbon atoms in the same region? These results are still too preliminary to give a definitive answer but, given more time, this would be one of the results that would be logically pursued given the current line of thought.

6.2.1 Oxide Reduction and Resulting Phenomena

This has been mentioned previously but it's worth repeating: the times at which new gases are introduced is only done once the previous gas has been evacuated from the chamber. In other words, transitioning from the annealing phase to growth phase, e.g. B139, first begins by closing the MFC valve of the O_2, waiting for the gas to be evacuated and the base pressure to be attained, and then inputting the appropriate gases. In this way we avoid any kind of gas mixing and possible reactions, e.g., CH_4, H_2 and O_2 to form water or CO_x, as well as any oxide reduction. It's been demonstrated this reduction still happens at these temperatures and pressures[97] but in a way that isn't manually controlled as it simply happens thermodynamically (Fig . 6-3). This line of thought is seen through certain experiments: for example B119 (large-area graphene growth) starts with an

O_2 anneal and ends with a H_2 anneal to assure that the copper surface was reduced prior to the growth phase. In previous experiments not reported here, a left over oxide dramatically slowed the growth down to such an extent that the doses required to initiate growth were much larger and thus raised fears of being in a completely different regime. Additionally, ending with H_2 helps counteract possible oxide-induced surface roughening which is touched upon later. This last idea is why, for example, B138 and B139 end with only a minute of O_2 so as to both keep the surface impurity-free and a formed oxide to a minimum. Both this sequencing of final gases in addition to time of exposure to an oxide reducer and its dose (in the form of H_2) adds an extra dimension to the complexity of the studies done here.

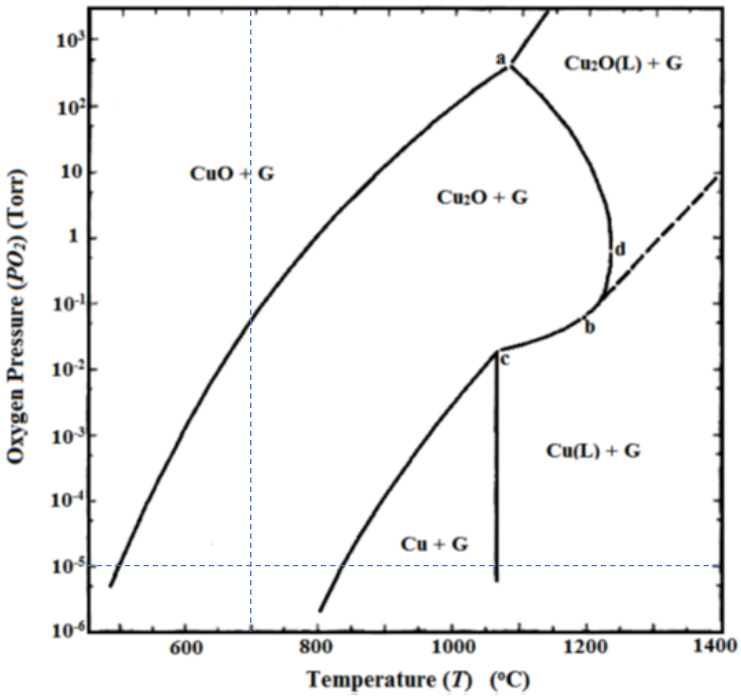

Figure 6-3 Copper-oxygen phase diagram. The intersection shown is the temperature and pressure chosen for this experiment. Reproduced with permission from ref. 93 Elsevier, copyright 1974.

There is yet another aspect of copper oxide formation which hasn't been touched upon which is its relation to surface roughening. Previous work[97] has shown that the reduction (via vacuum annealing) of Cu_2O roughens the surface through the creation of nano-indentations with a typical depth of $\sim 15nm$. Relatedly, the impact of surface roughness on an increased graphene

nucleation density is well established[70,98,99,100] and, while there hasn't been any research to demonstrate an explicit link between both (as far as the author of this document is aware), it seems intuitively clear that surface roughening due to copper oxide reduction would increase nucleation density. It is due to this that the last component (H_2 or O_2) of the anneal phase is relevant. By ending with O_2 we expect a diminished nucleation due to the oxide itself playing a role in quenching nucleation (from the O being liberated from the Cu_2O) which may be counteracted to some degree by an increase in nucleation due to surface roughness. In fact, this type of phenomena is likely what is seen in B124 after annealing in oxygen for 40 minutes which has not been observed in any other growth (Fig. 6-4).

Figure 6-4 B124 after 40 min anneal under $5x10^{-5}$ Torr O_2 and an attempted graphene growth. Marks highlighted in red, which only appear in this growth, may be indentations leftover from the oxide formation and reduction

6.3 **Crystallographic Orientation**

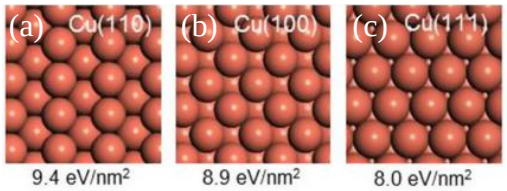

Figure 6-5 (a-c) showing structures and formation energies for (110), (100), and (111) of copper. Reproduced with permission from ref. 95. Elsevier, copyright 2017.

At the outset of these experiments the crystallographic orientation of the copper was never something that was in the crosshairs. However, enough information has emerged out of these growths to lend themselves to *suggesting* some trends. This analysis doesn't touch upon nucleation itself but, rather, upon a purported crystallographic impact of oxygen on both copper and graphene grains and the possibility of having crystallographically oriented graphene grains coalesce to form large area monocrystalline domains.

Some recent work has suggested that adding oxygen during the annealing phase restructures the polycrystalline copper crystallinity to Cu(111)[101,102] or Cu(100)[102,103] (Fig. 6-5). While the mechanisms aren't agreed upon in the literature (nor the preferred transition surface), a similar

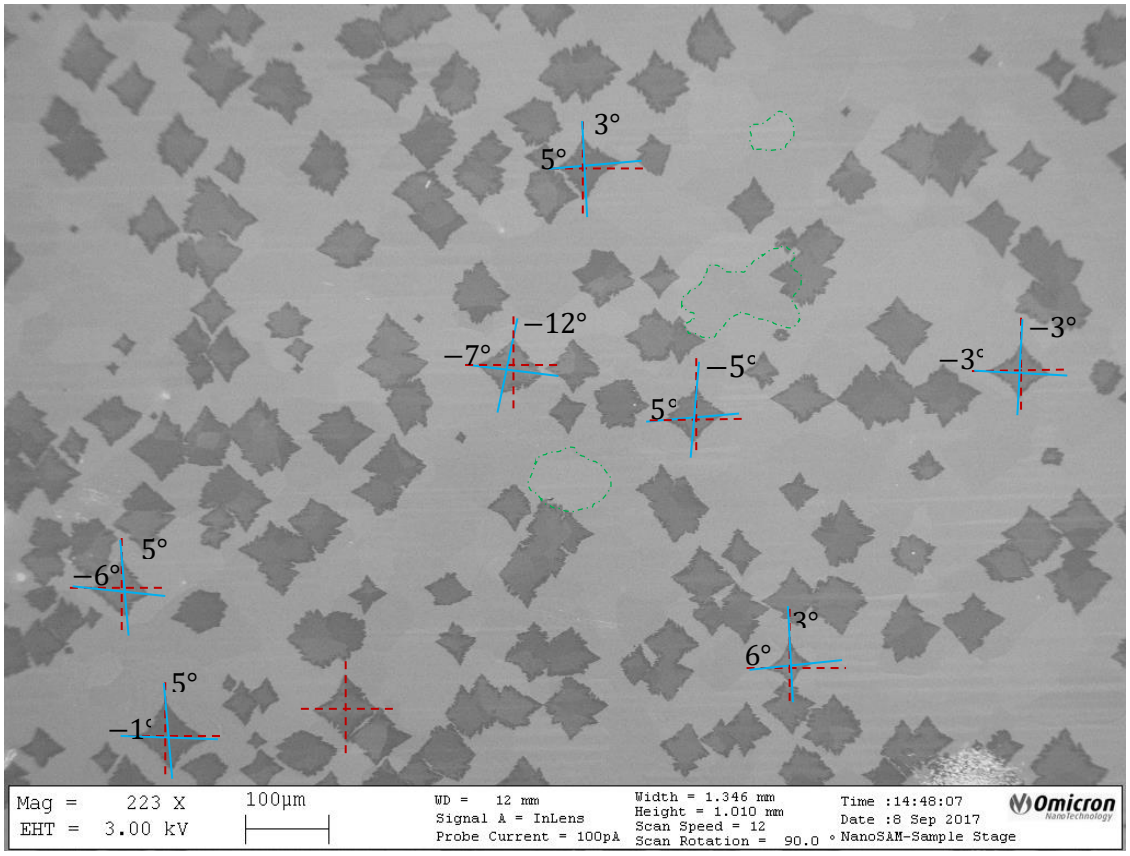

Figure 6-6 B119 showing well-aligned square-dominated graphene grains. red dotted showing vertical and horizontal baselines with blue lines showing offset from this baseline. Green dotted line highlighting some copper grains.

phenomenon seem to be at play in our growth. For example, in Fig. 6-6 a generally similar orientation of the graphene grains seems to be present. The degree of deviation (blue line) from the exact vertical and horizontal vary from $-12°$ to $5°$ and $-7°$ to $6°$, respectively, with the greatest difference between the horizontal and vertical being $11°$ from the small sample of graphene domains selected. Of interest is also the presence of observable underlying copper grains (green dotted outline). However, despite having many copper domains, the graphene domains all seem to be relatively well oriented suggesting that all these different copper domains likely share the same orientation. There are only 5 other articles that the author is able to find which have the same type of square-shaped graphene domains[103,104,105,106,107] with a near perfect $90°$ between the axes of growth. Due to this, one would expect the copper crystalline structure to either be Cu(100) or Cu(110) with the former less likely due to a missing-row configuration resulting in a higher formation energy (a Cu(111) structure has off-angles that wouldn't be conducive to this type of perpendicularly-oriented axes of growth as can be seen in Fig. 6-6). Except for the second one, all of these cited works identify the crystalline structure as Cu(100) while the second identifies these square domains as rectangular in nature and leans on other work[108] to attribute this shape to Cu(111). Nevertheless, all these works agree that this crystal structure reorganization follows from added oxygen in their pre-treatments which, with the proper amount of optimization, could play a role in growing large-area monocrystalline graphene.

Growth B121 (Fig. 6-7) lends itself to the same type of analysis, though, with no visibly underlying copper grains. These type of cross-like grains have been studied in a few different contexts[109,110,111] but seem to generally be much less prevalent in the literature with the first two of these studies being done *in-situ* in a LEEM with Cu(100) as the substrate, and the last study using polycrystalline copper with the graphene grains exhibiting this specific type of geometry on the Cu(100), solely.

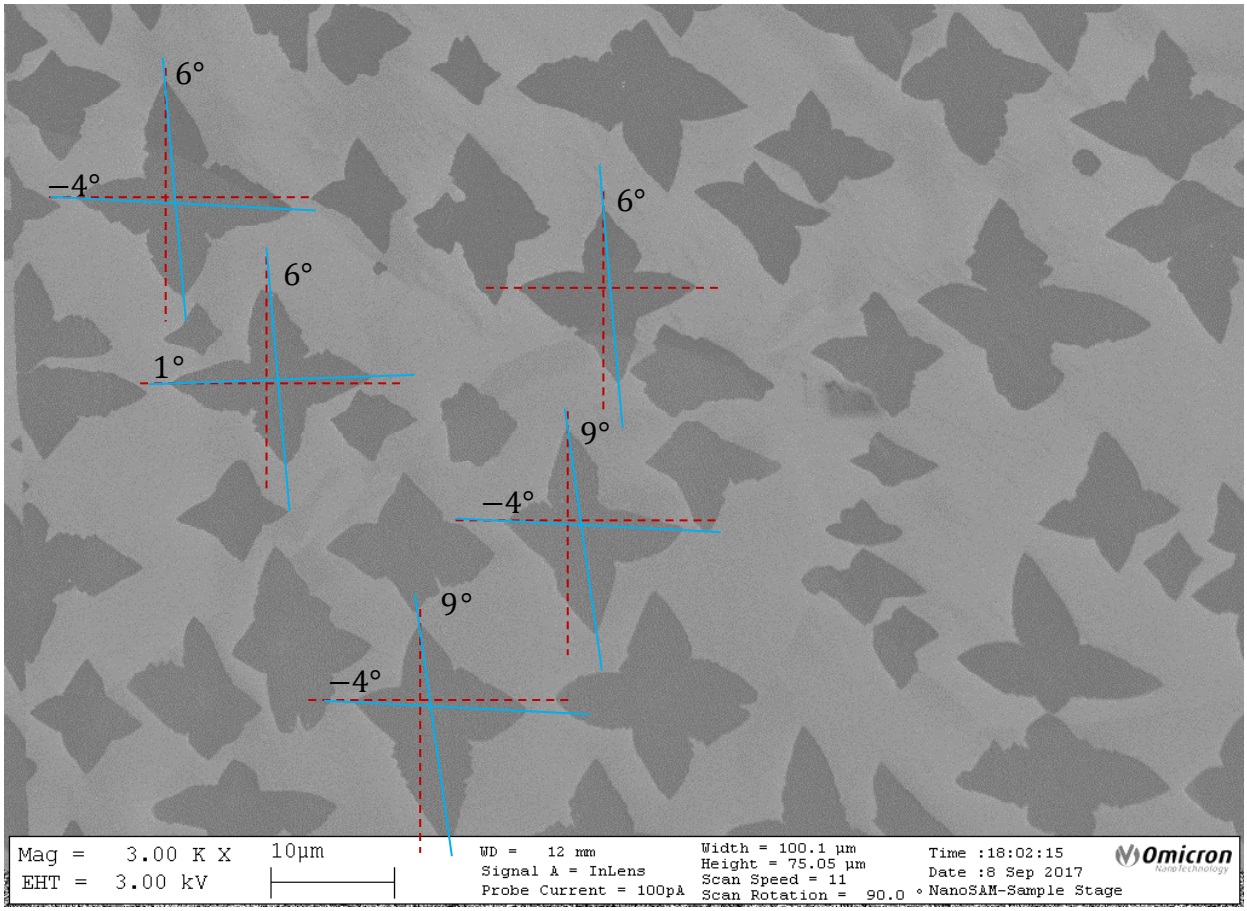

Figure 6-7 B121 showing well-aligned cross-like graphene grains. Red dotted showing vertical and horizontal baselines with blue lines showing offset from this baseline.

It is important to note an asterisk in the previous discussion concerning crystallographic orientation. The orientations that have been noted are the orientations of the copper solely and not that of the graphene grains. In the work by McCarty et al.[109,110] LEED was used to identify the exact orientations of the graphene itself (for the case of the cross-like geometry) which, while the axes of growth aligned with the [100] and [010] directions of copper, were actually along the <10> and <11>, which are the zigzag and exactly half-way between the zigzag and armchair directions, respectively. It is important to bring into view the picture being shown here: an optimization of the growth conditions using oxygen seems to have demonstrated in the literature as restructuring the copper crystallinity, which these results corroborate.

6.4 **Large-Grain**

At the outset of this project large-area graphene domains were the main focus. The largest area graphene obtained was done with both an oxidizing pre-treatment and, additionally, oxygen impurities added to the system during the growth phase. This last step was added in the form of argon diluted with 10ppm of O_2 which would put the growth approximately at the same O_2 content as other research groups not using purifiers for their gases (effectively reducing the impurities from the few ppm to ppb levels). Intuitively, the path to large-area graphene grains would be one of staying *just* below the necessary methane pressure to initiate nucleation hoping that statistically, at some location, enough carbon atoms would come together to serve as a nucleation center, enabling a full monocrystalline sheet of graphene. One way of "cheating" is by adding this oxygen into the gas mixture to effectively increase the necessary methane partial pressure for nucleation as well as reducing the rate of growth (something extensively studied by Choubak *et al.*[83,84] within the context of gas impurities). One impact of the added oxygen is immediately visible by the rough and uneven edges due to etching. Such a low graphene nucleation density is also an impact of the oxygen with these already large $80\ x\ 80 \mu m$ grains (Fig. 6-8 b)) having ample room to grow. Presumably the added oxygen impurities serve to keep the nucleation low by "burning" some of the smaller carbon clusters before they attain critical size to serve as a nucleation center. As was mentioned earlier, it's entirely plausible that leaving the oxide present, that is, not reducing it prior to initiating nucleation could slow nucleation even lower, yielding even larger grains. This work is preliminary but definitely paves the way for many different approaches to large-area graphene grains.

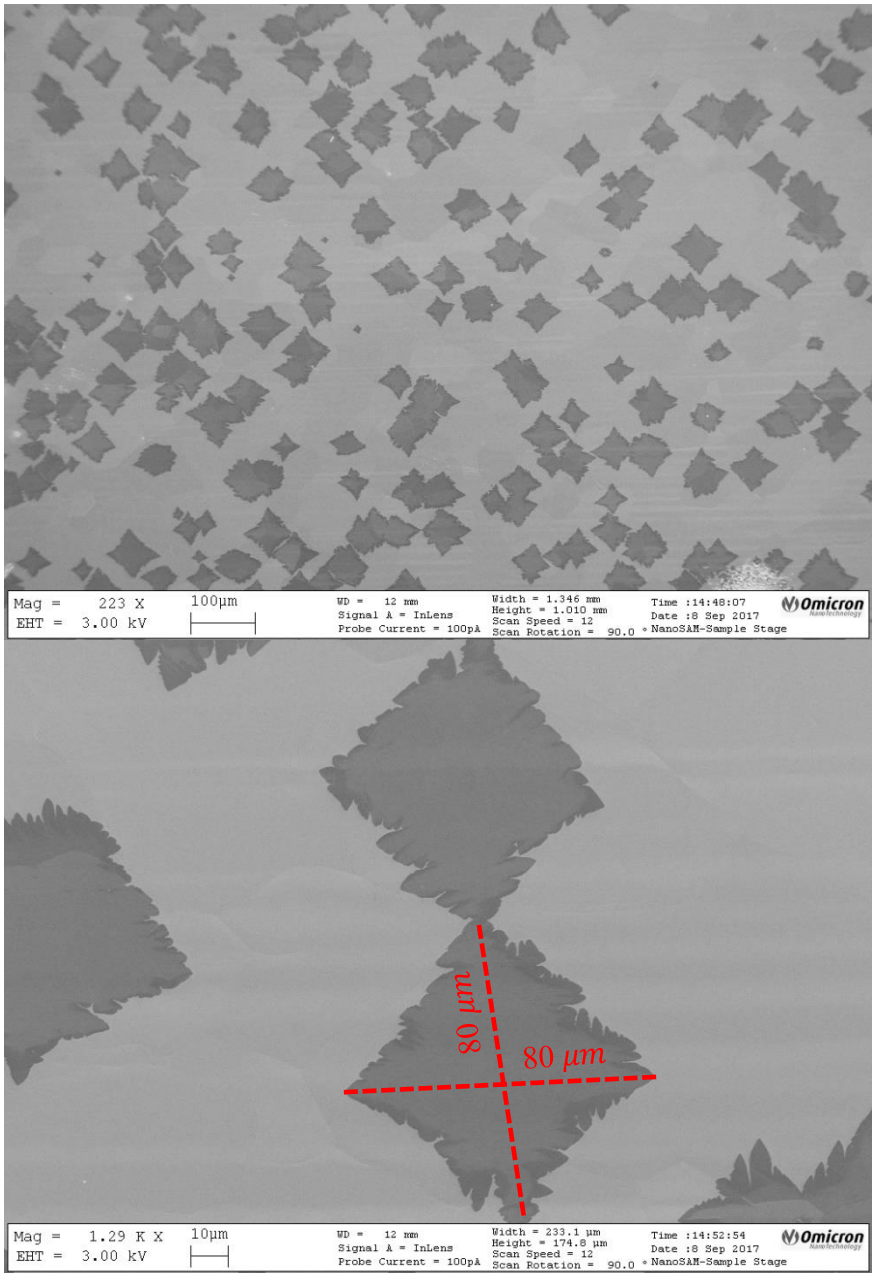

Figure 6-8 SEM micrograph of B119, the large area graphene growth. (a) A low coverage (due to low nucleation density) enables large area grains up to (b) 80x80 μm.

6.5 **Bi-/Multi-layers**

Despite having a much smaller dose than Choubak's growths, a completed layer was achieved with no bi/multilayers, attributed to the ridding of the carbonaceous impurities. Certainly, these results make sense given the explanations provided at the end of Chapter 2 in relation to the noted increase in bi- and multi- layers by Choubak *et al.* which connected their presence to the lack

of oxidizing impurities due to a highly purified environment. Due to our addition of oxidizing impurities we've been able to suppress their occurrence.

The data concerning bi- and multi- layers were also results that emerged from careful analysis of the SEM micrographs. It was noticed that the bilayer formation was quenched when an oxygen pre-treatment was done which helped wrap up, in our own minds, the mechanisms at play when considered alongside the other phenomenon we observed, in particular, the results from Choubak's thesis as well as her published work.

While there have been reports of bi-layers following a wedding-cake growth, it's generally accepted that most bilayers form in an inverted wedding-cake fashion, following from the idea that a substrate is necessary to aid in the dehydrogenation of methane, as mentioned in Chapter 1 and 2. Therefore, proceeding from an understanding that bilayers originate at the copper interface under the first graphene layer, an answer is still necessary to explain how the carbon manages to end up between the copper and the graphene. Our model proposed in Chapter 4 partially answers this elegantly and unexpectedly: the carbon responsible for the bi- and multi- layers originates from within the copper itself.

It's certainly true that there is no sign of bilayers in any of the partial growths present throughout this work, something not self-evident (i.e., partial growths can certainly exhibit beginnings of bilayers, in fact, some in the literature ascribe the growth of completed bilayers as a simultaneous growth of both layers[112]). However, to be consistent with past growths from within this research group to maintain a consistency in experimental setup we only presented full growths to better compare, from which no bilayers were observed either by inspection through SEM micrographs or spectroscopically. Therefore, it seems that by ridding the bulk carbonaceous impurities we also rid ourselves of the primary method by which graphene bilayers are formed.

CHAPTER 7 CONCLUSION AND PERSPECTIVES

The impact of oxygen on graphene nucleation was explored through three different series of experiments. Series 1, with the only differentiating parameter being 1 min O_2 annealing, resulted in a 21-fold decrease in nucleation density, from 0.59 to 0.028 μm^{-2} which resulted in a 10-fold increase in the average graphene size, from 1.1 to 11.76 μm^2. As a result, the total graphene coverage was halved, from 65% to 33%.

The second series of experiments demonstrated a viable route to enhancing the gettering action of oxygen via formation of a copper oxide by exploiting the copper-oxygen phase diagram. A consistent reduction in nucleation density, from 0.08 to 0.0045 μm^{-2} to complete quenching was achieved by doubling the time of oxygen anneal at $700°C$ from 10 min to 20 min and lastly 40 min. This resulted in an increase in average graphene size from 55.8 to 85.2 μm^2 to 0, respectively, with a graphene coverage consistent around ~39% for 10 and 20 min.

Lastly, we were able to leverage some of this new-found information to grow large-area graphene grains, enabling a low nucleation density of $1.4x10^{-4}$ μm^{-2}, resulting in an average size of 860 μm^2, with ample room to grow due to a graphene coverage of 28%.

That bulk-bound carbon in copper was never considered to play a role in graphene nucleation isn't so surprising considering its carbon solubility. What is surprising, and is highlighted throughout this work, is the extent to which it seems to dominate early-stage graphene synthesis *via* its impact on nucleation. Paying special attention to the oxygen-copper phase diagram a copper oxide was encouraged and was shown to increase the efficacy of the oxygen pre-treatment when done at $700°C$. By ridding the copper of deleterious carbon within the bulk *via* oxygen pre-treatment at $700°C$, a quenching of nucleation proportional to pre-treatment time at our usual methane partial pressures was accomplished. Due to this ridding of carbon, which could not migrate from the bulk to surface under the first layer, the removal of bilayers was also observed. Lastly, with an added partial pressure of oxygen during the growth phase large-area graphene grains were grown which was aided by the fact that the nucleations were proportional to the methane flux with no "incident" nucleations occurring due to out-diffusing carbonaceous impurities.

This preliminary work primarily serves as a roadmap for ideas to explore centered around the role of oxygen pre-treatments due to its role as a carbon getter. It demonstrated that additional pre-

treatment steps could be included to have a better control over CVD grown graphene. However, it did not confirm the form of the carbon found within the bulk, which it itself could answer certain questions. For example, if it's true that these clusters are graphitic by nature then either a mechanism would have to be elaborated that could explain why or how the carbon would congregate locally (perhaps carbon diffusing through the copper grain boundaries would encourage this sort of phenomena) or some external factor such as one that was proposed in the literature, i.e., due to the manufacturing and fabrication process of the cold-rolled copper foil. Nevertheless, the data coupled with our model suggests that the carbon found within the bulk is more than likely not atomic simply due to the length of time required to properly remove this, as demonstrated by the pre-treatment time required for a quenching of nucleation.

As mentioned above, this work merely served to pave the way for more interesting experiments and ideas:

- Find a relationship between time of oxygen pre-treatment at $700°C$ and methane partial pressure necessary to initiate nucleation.
- Compare these results to same parameters done on copper grown using atomic layer deposition to have a better sense of the origin of the carbonaceous impurities. Along the same lines, assuming single-crystalline copper growth, some information concerning copper grain boundaries could also be obtained.
- Continue along the same line with introduction of argon diluted with 10ppm of oxygen, i.e., increasing the argon partial pressure to be at the cusp of nucleation to yield even larger grains. Additionally, the same type of oxygen pre-treatment at $700°C$ should be explored with the diluted argon to yield even larger grains.
- Throughout these further growths, special attention should be payed to the presence of bilayers to further confirm the model.

It's difficult to know how far we are from having a fundamental control over graphene growth to propel ourselves into this so-called "graphene age". It's hoped that this work can be seen as a small drop in the pool of knowledge, certainly not making a big splash but perhaps some small waves will still come from it.

BIBLIOGRAPHY

1. May, R. & May, R. On the Atomic Weight o f Graphite. JBy. *Philos. Trans. R. Soc. London* **149,** 249–259 (1859).
2. Wallace, P. R. The Band Theory of Graphite. *Phys. Rev.* **71,** 622–634 (1947).
3. DiVincenzo, D. P. & Mele, E. J. Self-consistent effective-mass theory for intralayer screening in graphite intercalation compounds. *Phys. Rev. B* **29,** 1685–1694 (1984).
4. Geim, A. K. & Novoselov, K. S. The Rise of Graphene. *Nanosci. Technol. A Collect. Rev. from Nat. Journals* 11–19 (2010).
5. Schwierz, F. Graphene transistors. *Nat. Nanotechnol.* **5,** 487–496 (2010).
6. Raccichini, R., Varzi, A., Passerini, S. & Scrosati, B. The role of graphene for electrochemical energy storage. *Nat. Mater.* **14,** 271–279 (2015).
7. Wang, X., Zhi, L. & Müllen, K. Transparent, conductive graphene electrodes for dye-sensitized solar cells. *Nano Lett.* **8,** 323–327 (2008).
8. Secor, E. B., Prabhumirashi, P. L., Puntambekar, K., Geier, M. L. & Hersam, M. C. Inkjet printing of high conductivity, flexible graphene patterns. *J. Phys. Chem. Lett.* **4,** 1347–1351 (2013).
9. Stankovich, S. *et al.* Graphene-based composite materials. *Nature* **442,** 282–286 (2006).
10. Shao, Y. *et al.* Graphene based electrochemical sensors and biosensors: A review. *Electroanalysis* **22,** 1027–1036 (2010).
11. Novoselov, K. S. *et al.* Room-temperature electric field effect and carrier-type inversion in graphene films. *Science.* **306,** 660–662 (2004).
12. Balandin, A. A. *et al.* Superior thermal conductivity of single-layer graphene. *Nano Lett.* **8,** 902–907 (2008).
13. Lee, C., Wei, X., Kysar, J. W. & Hone, J. Measurement of the Elastic Properties and Intrinsic Strength of Monolayer Graphene. *Science.* **321,** 385–388 (2008).
14. Nair, R. R. *et al.* Fine Structure Constant Defines Visual Transperency of Graphene. *Science (80-.).* **320,** 2008 (2008).

15. Kim, K. S. *et al.* Large-scale pattern growth of graphene films for stretchable transparent electrodes. *Nature* **457,** 706–710 (2009).

16. Yu, Q. *et al.* Graphene segregated on Ni surfaces and transferred to insulators. *Appl. Phys. Lett.* **93,** 113103–21601 (2008).

17. Oshima, C. Ultra-thin epitaxial films of graphite and hexagonal boron nitride on solid surfaces. *J. Phys. Condens. Matter* **9,** 1–20 (1997).

18. Li, X. *et al.* Large-Area Synthesis of High-Quality and Uniform Graphene Films on Copper Foils. *Science.* **324,** 1312–1314 (2009).

19. Bhaviripudi, S., Jia, X., Dresselhaus, M. S. & Kong, J. Role of kinetic factors in chemical vapor deposition synthesis of uniform large area graphene using copper catalyst. *Nano Lett.* **10,** 4128–4133 (2010).

20. Guermoune, A. *et al.* Chemical vapor deposition synthesis of graphene on copper with methanol, ethanol, and propanol precursors. *Carbon N. Y.* **49,** 4204–4210 (2011).

21. Choubak, S., Biron, M., Levesque, P. L., Martel, R. & Desjardins, P. No graphene etching in purified hydrogen. *J. Phys. Chem. Lett.* **4,** 1100–1103 (2013).

22. Regmi, M., Chisholm, M. F. & Eres, G. The effect of growth parameters on the intrinsic properties of large-area single layer graphene grown by chemical vapor deposition on Cu. *Carbon N. Y.* **50,** 134–141 (2012).

23. Huang, X., Qi, X., Boey, F. & Zhang, H. CRITICAL REVIEW Chemical Society Reviews Graphene-based composites. *Chem. Soc. Rev. Chem. Soc. Rev* **41,** 525–944 (2012).

24. De Heer, W. A. *et al.* Epitaxial graphene. *Solid State Commun.* **143,** 92–100 (2007).

25. Batzill, M. & Weinberg, W. H. The surface science of graphene: Metal interfaces, CVD synthesis, nanoribbons, chemical modifications, and defects. *Surf. Sci. Rep.* **67,** 83–115 (2012).

26. Li, Z. *et al.* Low-Temperature Growth of Graphene by Chemical Vapor Deposition Using Solid and Liquid Carbon Sources. **5,** 3385–3390 (2011).

27. Kraus, J., Bobel, M. & Gunther, S. Suppressing graphene nucleation during CVD on polycrystalline Cu by controlling the carbon content of the support foils. *Carbon N. Y.* **96,**

153–165 (2016).

28. Levendorf, M. P., Ruiz-Vargas, C. S., Garg, S. & Park, J. Transfer-free batch fabrication of single layer graphene transistors. *Nano Lett.* **9,** 4479–4483 (2009).

29. Lee, Y. *et al.* Wafer-Scale Synthesis and Transfer of graphene films. *Nano Lett.* **10,** 490–3 (2010).

30. Ismach, A. *et al.* Direct chemical vapor deposition of graphene on dielectric surfaces. *Nano Lett.* **10,** 1542–1548 (2010).

31. Bae, S. *et al.* Roll-to-roll production of 30-inch graphene films for transparent electrodes. *Nat. Nanotechnol.* **5,** 574–578 (2010).

32. Reckinger, N. *et al.* Oxidation-assisted graphene heteroepitaxy on copper foil. *Nanoscale* **8,** 18751–18759 (2016).

33. Coraux, J., N'Diaye, A. T., Busse, C. & Michely, T. Structural coherency of graphene on Ir(111). *Nano Lett.* **8,** 565–570 (2008).

34. Sutter, P. W., Flege, J. I. & Sutter, E. A. Epitaxial graphene on ruthenium. *Nat. Mater.* **7,** 406–411 (2008).

35. Sutter, P., Sadowski, J. T. & Sutter, E. Graphene on Pt(111): Growth and substrate interaction. *Phys. Rev. B - Condens. Matter Mater. Phys.* **80,** (2009).

36. Kwon, S. Y. *et al.* Growth of semiconducting graphene on palladium. *Nano Lett.* **9,** 3985–3990 (2009).

37. Eom, D. *et al.* Structure and electronic properties of graphene nanoislands on CO(0001). *Nano Lett.* **9,** 2844–2848 (2009).

38. Seah, C.-M., Chai, S.-P. & Mohamed, A. R. Mechanisms of graphene growth by chemical vapour deposition on transition metals. *Carbon N. Y.* **70,** 1–21 (2014).

39. Okamoto, H., Schlesinger, M. E. & Mueller, E. M. ASM Handbook Volume 3: Alloy Phase Diagrams. **3,** 280–285 (2016).

40. Li, X., Cai, W., Colombo, L. & Ruoff, R. S. Evolution of graphene growth on Ni and Cu by carbon isotope labeling. *Nano Lett.* **9,** 4268–4272 (2009).

41. Kang, B. J., Mun, J. H., Hwang, C. Y. & Cho, B. J. Monolayer graphene growth on sputtered thin film platinum. *J. Appl. Phys.* **106,** 104309 (2009).

42. Selman, G. L., Ellison, P. J. & Darling, a. S. Carbon in Platinum and Palladium: Solubility determinations and diffusion at high temperatures. *Platin. Met. Rev.* **14,** 14–20 (1970).

43. López, G. A. & Mittemeijer, E. J. The solubility of C in solid Cu. *Scr. Mater.* **51,** 1–5 (2004).

44. Shu, H., Chen, X., Tao, X. & Ding, F. Edge Structural Stability and Kinetics of Graphene Chemical Vapor Deposition Growth. **6,** 3243–3250 (2012).

45. Li, X. *et al.* Graphene films with large domain size by a two-step chemical vapor deposition process. *Nano Lett.* **10,** 4328–4334 (2010).

46. Wang, X., Yuan, Q., Li, J. & Ding, F. The transition metal surface dependent methane decomposition in graphene chemical vapor deposition growth. *Nanoscale* **9,** (2017).

47. Zhang, Y. *et al.* Vapor trapping growth of single-crystalline graphene flowers: Synthesis, morphology, and electronic properties. *Nano Lett.* **12,** 2810–2816 (2012).

48. Kidambi, P. R. *et al.* The parameter space of graphene chemical vapor deposition on polycrystalline Cu. *J. Phys. Chem. C* **116,** 22492–22501 (2012).

49. Yao, Y. & Wong, C. P. Monolayer graphene growth using additional etching process in atmospheric pressure chemical vapor deposition. *Carbon N. Y.* **50,** 5203–5209 (2012).

50. Losurdo, M., Giangregorio, M. M., Capezzuto, P. & Bruno, G. Graphene CVD growth on copper and nickel: role of hydrogen in kinetics and structure. *Phys. Chem.* **13,** 20836–20843 (2083).

51. Vlassiouk, I., Regmi, M., Fulvio, P., Dai, S. & Smirnov, S. Role of Hydrogen in Chemical Vapor Deposition Growth of Large Single- Crystal Graphene. **5,** 6069–6076 (2011).

52. Choubak, S. *et al.* Graphene CVD: Interplay between growth and etching on morphology and stacking by hydrogen and oxidizing impurities. *J. Phys. Chem. C* **118,** 21532–21540 (2014).

53. Zhang, W., Wu, P., Li, Z. & Yang, J. First-Principles Thermodynamics of Graphene Growth on Cu Surfaces. *J. Phys. Chem. C* **115,** 17782–17787 (2011).

54. Li, Z. *et al.* Graphene thickness control via gas-phase dynamics in chemical vapor deposition. *J. Phys. Chem. C* **116,** 10557–10562 (2012).

55. Shu, H., Tao, X.-M. & Ding, F. What are the active carbon species during graphene chemical vapor deposition growth? *Nanoscale* **7,** 1627–1634 (2015).

56. Mi, X., Meunier, V., Koratkar, N. & Shi, Y. Facet-insensitive graphene growth on copper. *Phys. Rev. B* **85,** 155436 (2012).

57. Van Wesep, R. G., Chen, H., Zhu, W. & Zhang, Z. Communication: Stable carbon nanoarches in the initial stages of epitaxial growth of graphene on Cu(111). *J. Chem. Phys.* **134,** 1–5 (2011).

58. Xing, B., Pang, X. & Wang, G. C – H bond activation of methane on clean and oxygen pre-covered metals : A systematic theoretical study. *J. Catal.* **282,** 74–82 (2011).

59. Xing, B. & Wang, G.-C. Insight into the general rule for the activation of the X – H bonds (X = C, N, O, S) induced by chemisorbed oxygen atoms. *Phys. Chem.* **16,** 2621–2629 (2014).

60. Liang, T. *et al.* Graphene Nucleation Preferentially at Oxygen-Rich Cu Sites Rather Than on Pure Cu Surface. *Adv. Mater.* **27,** 6404–6410 (2015).

61. Xu, X. *et al.* Ultrafast growth of single-crystal graphene assisted by a continuous oxygen supply. *Nat. Nanotechnol.* **11,** 930–935 (2016).

62. Han, G. H. *et al.* Influence of copper morphology in forming nucleation seeds for graphene growth. *Nano Lett.* **11,** 4144–4148 (2011).

63. Gao, J., Yip, J., Zhao, J., Yakobson, B. I. & Ding, F. Graphene Nucleation on Transition Metal Surface: Structure Transformation and Role of the Metal Step Edge. *J. Am. Chem. Soc* **133,** 5009–5015 (2011).

64. Fan, L. *et al.* Correlation between nanoparticle location and graphene nucleation in chemical vapour deposition of graphene. *J. Mater. Chem. A* **2,** 13123–13128 (2014).

65. Ghosh, P. *et al.* Insights on Defect-Mediated Heterogeneous Nucleation of Graphene on Copper. *J. Phys. Chem. C* **119,** 2513–2522 (2015).

66. Dong Wang, P. *et al.* Facile growth of centimeter - sized single - crystal graphene on copper foil at atmospheric pressure. *J . Mater . Chem . C* **3,** 3503–3818

67. Hao, Y. *et al.* The role of surface oxygen in the growth of large single-crystal graphene on copper. *Science.* **342,** 720–723 (2013).

68. Chen, X. *et al.* Chemical vapor deposition growth of 5 mm hexagonal single-crystal graphene from ethanol. *Carbon N. Y.* **94,** 810–815 (2015).

69. Magnuson, C. W. *et al.* Copper oxide as a 'self-cleaning' substrate for graphene growth. *J. Mater. Res.* **29,** 403–409 (2014).

70. Miseikis, V. *et al.* Rapid CVD growth of millimetre-sized single crystal graphene using a cold-wall reactor. *2D Mater.* **2,** 014006 (2015).

71. Pang, J. *et al.* Oxidation as a means to remove surface contaminants on Cu foil prior to graphene growth by chemical vapor deposition. *J. Phys. Chem. C* **119,** 13363–13368 (2015).

72. Rakhshani, A. E. Preparation, characteristics and photovoltaic properties of cuprous oxide—a review. *Solid. State. Electron.* **29,** 7–17 (1986).

73. Abidi, I. H. *et al.* Regulating Top-Surface Multilayer/Single-Crystal Graphene Growth by "Gettering" Carbon Diffusion at Backside of the Copper Foil. *Adv. Funct. Mater.* **27,** 1–11 (2017).

74. Braeuninger-Weimer, P., Brennan, B., Pollard, A. J. & Hofmann, S. Understanding and Controlling Cu-Catalyzed Graphene Nucleation: The Role of Impurities, Roughness, and Oxygen Scavenging. *Chem. Mater.* **28,** 8905–8915 (2016).

75. Li, Q. *et al.* Growth of adlayer graphene on Cu studied by carbon isotope labeling. *Nano Lett.* **13,** 486–490 (2013).

76. Han, Z. *et al.* Homogeneous optical and electronic properties of graphene due to the suppression of multilayer patches during CVD on copper foils. *Adv. Funct. Mater.* **24,** 964–970 (2014).

77. Hao, Y. *et al.* Oxygen-activated growth and bandgap tunability of large single-crystal bilayer graphene. *Nat. Nanotechnol.* **11,** 426–431 (2016).

78. Liu, L. *et al.* High-Yield Chemical Vapor Deposition Growth of High-Quality Large-Area AB-Stacked Bilayer Graphene. **6,** 8241–8249 (2012).

79. Habib, M. R. *et al.* A review of theoretical study of graphene chemical vapor deposition

synthesis on metals: nucleation, growth, and the role of hydrogen and oxygen. (2018).

80. Wu, P., Zhai, X., Li, Z. & Yang, J. Bilayer graphene growth via a penetration mechanism. *J. Phys. Chem. C* **118,** 6201–6206 (2014).

81. Li, J. *et al.* Impurity-induced formation of bilayered graphene on copper by chemical vapor deposition. *Nano Res.* **9,** 2803–2810 (2016).

82. Dong Wang, C., Wan, L.-J., Li, J. & Dong Wang, ab. Unexpected functions of oxygen in a chemical vapor deposition atmosphere to regulate graphene growth modes. *Chem. Commun. Chem. Commun* **51,** 15475–15602 (2015).

83. Choubak, S., Biron, M., Levesque, P. L., Martel, R. & Desjardins, P. No graphene etching in purified hydrogen. *J. Phys. Chem. Lett.* **4,** 1100–1103 (2013).

84. Choubak, S. *et al.* Graphene CVD: Interplay between growth and etching on morphology and stacking by hydrogen and oxidizing impurities. *J. Phys. Chem. C* **118,** 21532–21540 (2014).

85. Zhang, Y., Li, Z., Kim, P., Zhang, L. & Zhou, C. Anisotropic hydrogen etching of chemical vapor deposited graphene. *ACS Nano* **6,** 126–132 (2012).

86. Kurt J. Lesker Company | KF (QF) Flange Technical Notes | Vacuum Science Is Our Business. Available at: https://www.lesker.com/newweb/flanges/flanges_technicalnotes_kf_1.cfm. (Accessed: 11th December 2017)

87. G&et, C., Daroux+, M. & Billaudi, F. Methane pyrolysis: thermodynamics. *Pergamon Chemcol Eng. Sci.* **52,** 815–827 (1997).

88. K. L. Chavez and D. W. Hess. A Novel Method of Etching Copper Oxide Using Acetic Acid. *J. Electrochem. Soc.* **148,** G640–G643 (2001).

89. Goldstein, J. I. *et al. Scanning Electron Microscopy and X-ray Microanalysis*. (Kluwer Academic/Plenum Publishers, 2003). doi:10.1007/978-1-4615-0215-9

90. Spallas, J. X. and J. P. Different Contrast Mechanisms in SEM Imaging of Graphene. *Agil. Technol.* 1–8 (2012).

91. Ferrari, A. C. *et al.* Raman spectrum of graphene and graphene layers. *Phys. Rev. Lett.* **97,**

(2006).

92. Tuinstra, F. & Koenig, J. L. Raman Spectrum of Graphite. *J. Chem. Phys.* **53,** 1126–1130 (1970).

93. Malard, L. M., Pimenta, M. A., Dresselhaus, G. & Dresselhaus, M. S. Raman spectroscopy in graphene. *Phys. Rep.* **473,** 51–87 (2009).

94. Schneider, C. A., Rasband, W. S. & Eliceiri, K. W. NIH Image to ImageJ: 25 years of image analysis. *Nat. Methods* **9,** (2012).

95. Schmidt-Whitley, R. D., Martinez-Clemente, M. & Revcolevschi, A. Growth and microstructural control of single crystal cuprous oxide Cu2O. *J. Cryst. Growth* **23,** 113–120 (1974).

96. Choubak, S. The Impact of Hydrogen and Oxidizing Impurities in Chemical Vapor Deposition of Graphene on Copper. (2015).

97. Zhou, G. & Yang, J. C. Reduction of Cu2O islands grown on a Cu(100)surface through vacuum annealing. *Phys. Rev. Lett.* **93,** 1–4 (2004).

98. Kim, H. *et al.* Activation Energy Paths for Graphene Nucleation and Growth on Cu. **6,** 3614–3623 (2012).

99. Luo, Z. *et al.* Effect of Substrate Roughness and Feedstock Concentration on Growth of Wafer-Scale Graphene at Atmospheric Pressure. | *Chem. Mater* **23,** 1441–1447 (2011).

100. Vlassiouk, I. *et al.* Large scale atmospheric pressure chemical vapor deposition of graphene. *Carbon N. Y.* **54,** 58–67 (2013).

101. Xu, X. *et al.* Ultrafast epitaxial growth of metre-sized single-crystal graphene on industrial Cu foil. *Sci. Bull.* **62,** 1074–1080 (2017).

102. Hu, J. *et al.* Roles of Oxygen and Hydrogen in Crystal Orientation Transition of Copper Foils for High-Quality Graphene Growth. *Sci. Rep.* **7,** 45358 (2017).

103. Wang, H. *et al.* Surface Monocrystallization of Copper Foil for Fast Growth of Large Single-Crystal Graphene under Free Molecular Flow. *Adv. Mater.* **28,** 8968–8974 (2016).

104. Wang, H. *et al.* Controllable synthesis of submillimeter single-crystal monolayer graphene

domains on copper foils by suppressing nucleation. *J. Am. Chem. Soc.* **134,** 3627–3630 (2012).

105. Ren, H. *et al.* Rapid growth of angle-confined large-domain graphene bicrystals. *Nano Res.* **10,** 1189–1199 (2017).

106. Gui-Ping Dai , Marvin H. Wu, D. K. T. & K. V. Square-Shaped, Single-Crystal, Monolayer Graphene Domains by Low-Pressure Chemical Vapor Deposition. *Mater. Res. Lett.* **1,** 67–76 (2013).

107. Chen, Q. *et al.* Synthesis of well-aligned millimeter-sized tetragon-shaped graphene domains by tuning the copper substrate orientation. *Carbon N. Y.* **93,** 945–952 (2015).

108. Wu, Y. A., Robertson, A. W., Sch€, F., Speller, S. C. & Warner, J. H. Aligned Rectangular Few-Layer Graphene Domains on Copper Surfaces. *Chem. Mater* **23,** 4543–4547 (2011).

109. Wofford, J. M., Nie, S., Thurmer, K., McCarty, K. F. & Dubon, O. D. Influence of lattice orientation on growth and structure of graphene on Cu(001). *Carbon N. Y.* **90,** 284–290 (2015).

110. Wofford, J. M., Nie, S., McCarty, K. F., Bartelt, N. C. & Dubon, O. D. Graphene islands on Cu foils: The interplay between shape, orientation, and defects. *Nano Lett.* **10,** 4890–4896 (2010).

111. Jung, D. H., Kang, C., Nam, J. E., Jeong, H. & Lee, J. S. Surface Diffusion Directed Growth of Anisotropic Graphene Domains on Different Copper Lattices. *Sci. Rep.* **6,** (2016).

112. Liu, Q., Gong, Y., Wilt, J. S., Sakidja, R. & Wu, J. Synchronous growth of AB-stacked bilayer graphene on Cu by simply controlling hydrogen pressure in CVD process. *Carbon N. Y.* **93,** 199–206 (2015).

APPENDIX: MODEL DERIVATION

In this section we mathematically elucidate the basis of the model. We work our way to demonstrating the higher "purifying power" by formation of $Cu_2O\ via$ oxidation at $700°C$, giving a lower bound of copper-bulk carbon content and demonstrating that the carbonaceous inclusions must be in amorphous or graphitic form (in any case, in a form more stable than atomic carbon), along the way.

We first begin by estimating an upper limit on the pre-treatment time. We suppose that the copper is a semi-infinite 1D bar with an initial carbon concentration of C_{0c} where the O_2 keeps the surface carbon concentration C_C equal to 0. From the diffusion equation's general solution we obtain:

$$c(x,t) = A + B \cdot \mathrm{erf}\left(\frac{x}{2\sqrt{D \cdot t}}\right) \tag{A.1}$$

setting boundary conditions

$$c(0,t) = 0 \tag{A.1a}$$

$$c(\infty,t) = C_{0C} \tag{A.1b}$$

$$c(x,0) = C_{oC} \tag{A.1c}$$

which yields

$$c(0,t) = 0 \rightarrow A = 0 \tag{A.1d}$$

$$c(x,0) = C_{0C} \rightarrow B = C_{0C} \tag{A.1e}$$

therefore

$$c(x,t) = C_{0C} \cdot \mathrm{erf}\left(\frac{x}{2\sqrt{D \cdot t}}\right) \tag{A.2}$$

$$x = 2\sqrt{D \cdot t} \cdot \text{erf}^{-1} \frac{C(?,3600s)}{C_{0C}} \tag{A.3}$$

$$= 2\sqrt{1.26x10^{-10} \cdot 3600} \cdot \text{erf}^{-1}(1x10^{-3}) \tag{A.3a}$$

$$= 1.2\ \mu m$$

is the depth at which the carbon concentration will have diminished by 3 orders of magnitude with respect to the initial carbon concentration, i.e.,

$$\frac{C_C}{C_{0C}} < 1x10^{-3} \tag{A.4}$$

after 60 minutes, which is the amount necessary to reduce the nucleation density by $1x10^6$.

7.1.1 Surface Segregation and Nucleation

We first calculate the necessary amount of copper evaporated for nucleation to occur given the carbon content estimated to be between 0.5 and 200 ppm.[27]

$$L_{Cu} \cdot \overline{n_{Cu}} \Big/ \overline{d_{Cu}} \cdot impurity\ ratio = 5x10^{13} \frac{atoms}{cm^2} \tag{A.5}$$

where

$$\overline{d_{Cu}} = 0.228\ nm \tag{A.6}$$

is the effective inter-planar distance and

$$\overline{n_{Cu}} = \left(\frac{1}{\overline{d_{Cu}}}\right)^2 = 1.93x10^{15} \frac{atoms}{cm^2} \tag{A.7}$$

is the copper surface density. Solving (5) for L_{Cu} with the values of (6) and (7) yields a required evaporation between 0.025 and 11 μm for 240 ppm and 0.5 ppm of impurity, respectively.

From Clausius-Clapeyron

$$P_{Cu}(1000°C) = 8.22x10^{-5}\ mbar \tag{A.8}$$

and

$$Z_{Cu} = 7.6x10^{15}\ cm^{-2}s^{-1}. \tag{A.9}$$

Using a thin-film approximation we can estimate evaporation time as

$$t_{nucl} = \frac{c_{Cu}L_{Cu}}{Z_{Cu}} \tag{A.10}$$

which yields, for different impurity concentrations,

$$t_{nucl}^{0.5ppm} = 220\ \text{min} \tag{A.10a}$$

and

$$t_{nucl}^{240ppm} = 30\ s. \tag{A.10b}$$

This model does not hold for the lower carbon concentration as the nucleation time is longer than the growth time with half the sample being evaporated before nucleation, however, it could be conceivable for the higher carbon concentration.

The most realistic model follows from a finite geometry with a finite carbon concentration. Taking the depth solely, making the problem 1D, with a copper of thickness L and starting carbon concentration C_{0c}.

Starting from the diffusion equation

$$\frac{\partial}{\partial t}c = D\frac{\partial^2}{\partial x^2}c(x,t) \tag{A.11}$$

Using boundary conditions

$$c(x,0) = c_{0C} \tag{A.11a}$$

$$c(0,t) = c(L,t) = 0 \tag{A.11b}$$

The general solution corresponds to the homogeneous Dirichlet in 1D.

$$c(x,t) = \sum_{n=1}^{L} B_n \sin\left(\frac{n\pi x}{L}\right) e^{-\left(\frac{n\pi}{L}\right)^2 D\cdot t} \tag{A.12}$$

where

$$B_n = \frac{2}{L}\int_0^L c_s \sin\left(\frac{n\pi x}{L}\right) dx \qquad (A.12a)$$

$$= \frac{2c_s}{n\pi}(1-(-1)^n) \qquad (A.12b)$$

Using n=1 we have

$$c_1\left(\frac{L}{2}, t\right) = B_1 \sin\left(\frac{\frac{\pi L}{2}}{L}\right) e^{-\left(\frac{\pi}{L}\right)^2 D\cdot t}. \qquad (A.12c)$$

Solving for t

$$t = -\ln\left(\frac{\pi}{4}\frac{c_1}{c_s}\right)\cdot\left(\frac{L}{\pi}\right)^2 \cdot \frac{1}{D_C} \qquad (A.13)$$

$$= -\ln\left(\frac{\pi}{4}10^{-3}\right)\cdot\left(\frac{25x10^{-6}m}{\pi}\right)^2 \cdot \frac{\pi}{1.26x10^{-10}m^2} \qquad (A.14)$$

$$= 3.6s$$

Where the diffusion coefficient of carbon was calculated from

$$D = D_0 e^{-\left(\frac{E_A}{k_b T}\right)} \qquad (A.15)$$

using

$$D_0 = 5.55x10^{-7} m^2/s \qquad (A.16)$$

and the activation energy

$$E_A = 0.92\ eV \qquad (A.17)$$

for carbon which yields

$$D_C = 1.26x10^{-10}\ m^2/s \qquad (A.18)$$

This 3.6 s is the necessary amount of time for the desired purification of $\frac{C_C}{C_{0C}} < 1x10^{-3}$to take place due to the diffusion of carbon atoms.

The variation of the first term with respect to time, assuming uniformity of carbon in the thin film (as being 240 ppm), is given by

$$\frac{d}{dt}c_1\left(\frac{L}{2},t\right) = \left(\frac{4}{\pi}\right)\frac{d}{dt}c_s e^{-\left(\frac{\pi}{L}\right)^2 D\cdot t} \quad (A.19)$$

$$= -\frac{4\pi c_s}{L^2} D e^{-\left(\frac{\pi}{L}\right)^2 D\cdot t} \quad (A.20)$$

$$\frac{dn_c}{dt} = \frac{d}{dt}C_{Cu}\cdot imp\cdot\frac{L}{2} = -\frac{4\pi c_s}{L^2} D\cdot e^{-\left(\frac{\pi}{L}\right)^2 D\cdot t}\cdot imp\cdot\frac{L}{2} \quad (A.21)$$

Where L/2 is due to the copper evaporating from both sides equally. Setting t=0, we have

$$\frac{dn_c}{dt} = \frac{d}{dt}C_{Cu}\cdot imp\cdot\frac{L}{2} = -\frac{4\pi c_s}{L^2} D\cdot imp\cdot\frac{L}{2} \quad (A.22)$$

where C_{Cu} is the density of copper, which yields

$$\frac{dn_c}{dt} = 6.5x10^{12}/cm^2\,. \quad (A.23)$$

From the general expression relating gas pressure and collision frequency

$$Z_P = \frac{p}{\sqrt{2\pi m k_b T}} \quad (A.24)$$

at $1x10^{-5}\ Torr$ oxygen pressure we obtain

$$Z_{O_2} = 1.74x10^{15}/cm^2\,. \quad (A.25)$$

The probability P of impinging upon surface adsorbed carbon is

$$P = Z_{O_2}\cdot imp = 4.18x10^{11}/cm^2 \quad (A.26)$$

Therefore, there is not enough collision directly with the carbon to remove it from the surface even if the reaction rate was unitary, which means that the boundary condition could not be respected in this model, so that the purification time of copper by oxygen might be above this threshold.

7.1.2 **Collision-Rate Limited**

From the previous results, we see that the removal of the carbon is limited by the collision rate. Now we approximate that the copper is homogenised instantly so that C_c is uniform throughout the copper foil, which will also be true at the surface so that

$$imp = \frac{C_C}{C_{Cu}} \tag{A.26}$$

and

$$C_{Cu} = \frac{\rho_{Cu}}{M_{Cu}} \tag{A.27}$$

The number of carbon atoms removed per unit time will be proportional to the O_2 impingement rate times the probability of hitting a carbon atom (as opposed to a copper atom) which is given by the molar concentration of carbon divided by the molar density of copper c_s/c_{Cu}.

We can consider the removal rate as follows given a number N of carbon removed per area A

$$\frac{dN_c}{dt} = -f \cdot Z_{O_2} \cdot A \cdot \frac{c_C}{c_{Cu}} \tag{A.28}$$

where f is the collision efficiency and is estimated to be $f = 0.01$, and

$$\frac{N_c}{A} = C_c \lambda_r, \tag{A.29}$$

where λ_r is the reaction length which can be estimated to be equal to the Cu unit cell $\overline{d_{Cu}}$. Combining these, the expression can be rewritten as

$$\frac{dc_c}{dt} = \frac{f Z_{O_2}}{\overline{d_{Cu}}} \frac{c_C}{c_{Cu}}, \tag{A.30}$$

which can be solved to give

$$c_C(t) = c_C(0) e^{-\frac{f Z_{O_2}}{\overline{d_{Cu}} c_{Cu}} t} \tag{A.30a}$$

which gives us a time of

$$t = 12.8\,min \qquad (A.31)$$

to purify the copper. This is closer to the experimentally determined time of 60 min. Either the carbon content is greater or f is overestimated.

7.1.3 **Diffusion Competition**

In the previous approximation, despite the time found being of the same order as the experimental time we've observed, the carbon quantity in the copper seems too elevated for a simple C-Cu solution. Therefore, we suspect that there are carbonaceous inclusions within the copper bulk in addition to dissolved atomic carbon such that during the O_2 purification, the oxygen diffuses into the copper bulk and reacts with carbon into smaller fragments until it dissolves and then segregates to the surface and form gaseous CO.

By optimising the purification pre-treatment, we observed that oxidizing at $700°C$ instead of $1000°C$ reduces the nucleation density by a factor of 10 (for the same gas pressures and time). This is due to the fact that a cuprous oxide is formed at $700°C$, as can be seen in Cu-O phase diagram (Fig. 4.1), given by an oxygen concentration of

$$[O] = 0.33, \qquad (A.32)$$

which will diffuse with a coefficient

$$D_0(700°C) = 5x10^{-10} m^s/s\,. \qquad (A.33)$$

At $1000°C$ the oxygen concentration can be evaluated as

$$\frac{n}{V} = \frac{P}{RT} = 8x10^{10}\,\frac{O_2}{cm^3}. \qquad (A.34)$$

If we compare this to the number of copper atoms per unit volume,

$$C_{Cu} = 8x10^{22} Cu/cm^3\,, \qquad (A.35)$$

we obtain an impurity ratio of

$$0.001\ ppb\ O_2 \qquad (A.36)$$

at the surface. At this temperature

$$D_0(1000°C) = 3x10^{-9} m^2/s\,. \qquad (A.37)$$

Calculating the oxygen concentration at $700°C$ gives

$$[O]_{700°C} = 0.33 \cdot 8x10^{22}\, O_2/cm^3 \qquad (A.38)$$

$$[O]_{700°C} = 2.64x10^{22}\, O_2/cm^3 \qquad (A.38a)$$

Considering this problem to be a Dirichlet problem we have

$$\frac{dc_0}{dt} \propto C_{0O} \cdot D. \qquad (A.39)$$

Therefore, despite losing an order of magnitude in flux due to the decrease in D, we gain 11 orders of magnitude due to the formation of an oxide at the surface by diminishing the temperature to $700°C$.

To summarize: Given previously reported copper carbon content, 0.5 – 240ppm, the substrate would need to evaporate between 11 and $0.025\ \mu m$ which would take between 30 s and 220 min, respectively. This gives some sense of the carbon impurity present. The amount of time required to reduce the carbon concentration by 3 orders of magnitude at the center of the substrate is 3.6 s. A lower bound on the amount of time necessary to reduce the carbon concentration by 3 orders of magnitude is found to be 3.6 s. This would be consumed at a rate of $6.5x10^{12}/cm^2$, however, due to the impingement rate of oxygen, at $5x10^{-5}\ Torr$, yielding a probability of $4.18x10^{11}/cm^2$. Hence, there would not be enough collision directly with the carbon to remove it (given the best possible conditions of a unitary reaction rate) thus, again, only being a lower bound on the effective time necessary. Given that the consumption of carbon will be collision-rate limited, assuming a reaction coefficient $f = 0.01$, we calculate, for homogenized carbon impurities, a time of 12.8 min to purify the copper to the desired levels. Due to this time being shorter than the experimentally determined values, we propose that the carbon must be in graphitic form (referred to as carbonaceous inclusions). Therefore, we devise a more efficient way of purifying the copper substrate by exploiting the Cu-O phase diagram and annealing under O_2 at $700°C$ instead of $1000°C$, where an oxide layer, CuO_2, remains stable. *Via* this method we are able to increase by 11-fold the concentration of oxygen at the surface.